Journal of Engineering Physics and Thermophysics, Vol. 66, No. 1, 1994

HYDRODYNAMICS OF RISING BUBBLES AND DROPS

(REVIEW)

P. K. Volkov

UDC 532.529.6

INTRODUCTION

There is hardly a technology which does not use media with different kinds of inclusions: bubbles, drops, particles. Bubbles and drops rising in liquids assume different shapes. Visualization of flows reveals their different types: laminar, separationless; those involving the formation of a toroidal vortex at the rear; a vibrating bubble or drop with a kind of Kármán street behind it; a bubble or drop rising helically; a bubble in the form of a spherical cup with a large vortex; a drop concave at the front, etc. The problem of describing the laws that govern the rise of bubbles and drops has been covered extensively in the literature, both experimental and theoretical. Above all, the long and continuous interest in these problems is due to the fact that they underlie the description of the interaction of two-phase media. Despite the long history of intense study for the past forty years, there is as yet no satisfactory description of the motion of different media and hebavior of mixtures as a whole (except for homogeneous models). One of the reasons for this in the theory of multiphase media is the absence of a complete picture of the interaction of rising (moving in a flow) individual formations with the carrier medium and with each other. These problems are very complicated and difficult to investigate theoretically. Apart from the obvious difficulty posed by the necessity to determine both the flow structure and the shape of bubbles and drops, they involve one other unknown quantity, i.e., the velocity of rise (the velocity of the relative motion of a separate particle in a liquid flow). This imposes additional constraints on obtaining information that would adequately take account of the process of rising. For example, a small and light solid sphere rises in a liquid with a single velocity, whereas the problem of flow around this sphere can be solved for any incident stream velocities. The situation is made much more complex if the shape of the surface changes with the flow hydrodynamics. Accounting for the inertia effects of moving particles is important in problems with external influences on the liquid (rise in a rotating liquid, electrically conducting liquid, etc.). On the theoretical level, up to now studies have generally been confined to the problems of flow past objects. The question concerning the compliance of these solutions with the problems of rise needs further study.

The available theoretical publications are concerned with various limiting cases of large (small) values of the problem parameters when a bubble (drop) has the shape of a sphere or ellipsoid. The present state of the subject is covered rather adequately in [1, 2]. However, asymptotic methods are unsuitable for the intermediate values of the parameters. Here, only a direct numerical calculation of the motion equations enables one to obtain information about the rising particles. This work aims at presenting the hydrodynamics of rising bubbles and drops and correlating the available data. Necessary comparisons are made between theoretical, numerical, and test data. Charts of flow modes are constructed; it is shown that the Laplace capillary constant is an important characteristic for the process of rise of bubbles and drops. The work is a natural complement to the available detailed reviews [3, 4] devoted to bubbles and drops. As a rule, the mathematical simulation is carried out within the framework of ideal and viscous liquids. The theoretical statements are not new. Investigations of the existence and uniqueness of solutions for a number of free-surface problems were conducted in [5-7]. It should be noted that the successes in the construction of numerical algorithms for solving Euler and Navier-Stokes equations with a free boundary are

Institute of Thermophysics, Siberian Branch of the Russian Academy of Sciences, Novosibirsk. Translated from Inzhenerno-Fizicheskii Zhurnal, Vol. 66, No. 1, pp. 93-123, January, 1994. Original article submitted August 5, 1993.

1062-0125/94/6601-0085$12.50

due largely to the theoretical investigations conducted, which constantly remind us that everything will come out fine.

Chapter 1. MODEL OF AN IDEAL LIQUID

1.1. Statement of the problem

The first exact solution to the problem of the dynamics of a spherical bubble is given in [8]. With allowance for spherical symmetry in the absence of gravity, the problem is reduced to the determination of the bubble radius as a function of the difference in pressure on the inside and at infinity. The change in the radius with time is given by a quadrature.

The complete statement of the problem concerning the rise of a bubble in a heavy infinite liquid was first made by Ovsyannikov [5]. Assuming the gas in the bubble to be inviscid and non-heat-conducting, its state can be described by one constant, i.e., by the thermodynamic pressure p_g. The liquid motion is described by the Euler equations which, for the potential φ in the axysymmetric case in a spherical coordinate system with the origin at the "bubble center," have the form

$$\Delta\varphi = 0\,, \tag{1.1}$$

$$\frac{\partial\varphi}{\partial t} + \frac{1}{2}\,|\nabla\varphi|^2 + \frac{p}{\rho} - gr\cos\theta = c\,(t)\,. \tag{1.2}$$

At infinity the liquid moves with a given velocity u

$$\varphi \to ur\cos\theta \quad \text{when} \quad r \to \infty\,. \tag{1.3}$$

The symmetry conditions are

$$\partial\varphi/\partial\theta = 0 \quad \text{when} \quad \theta = 0\,,\ \pi\,. \tag{1.4}$$

Moreover, on the free surface the kinematic and dynamic conditions should be fulfilled

$$-\frac{\partial R}{\partial t} + \frac{\partial\varphi}{\partial r} - \frac{1}{R^2}\,\frac{\partial\varphi}{\partial\theta}\,\frac{\partial R}{\partial\theta} = 0\,, \tag{1.5}$$

$$p_g = p + \sigma K\,. \tag{1.6}$$

The initial conditions should be prescribed only on the surface Γ:

$$t = 0\,,\ R\,(\theta\,,\ 0) = R_0\,,\ \varphi\,(\theta\,,\ 0) = \varphi_0\,. \tag{1.7}$$

Here t is the time; u is the liquid velocity at infinity; ρ is the liquid density; g is the acceleration of gravity; σ is the coefficient of surface tension; $r = R(\theta, t)$ is the equation of the free surface Γ; p is the pressure; K is the curvature of the surface Γ; $c(t)$ depends on the problem to be solved. For small rising times we may assume that the liquid at infinity is at rest: $\partial\varphi/\partial t \to 0$ when $r \to \infty$. Then $p_\infty/\rho - gr\cos\theta = c(t)$, and since p_∞ is independent of t (the liquid is at rest), what remains is $c(t) = p_0/\rho = \text{const}$, where p_0 is the additional pressure at infinity, which will be the parameter of the problem.

1.2. Unsteady-state rise of a bubble

The presence of gravity in the case of potential liquid flow makes the problem nonstationary, since it is impossible to compensate the effect of gravity force because of d'Alembert's paradox. In Eq. (1.6) the capillary

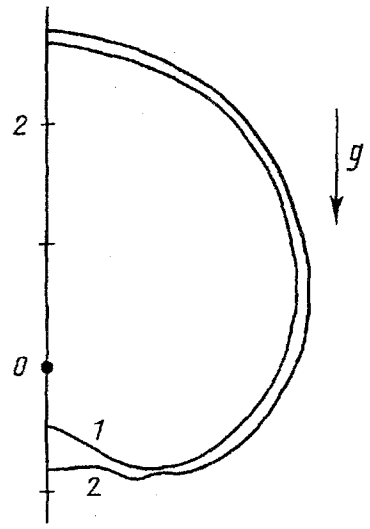

Fig. 1. The bubble shape obtained by different techniques: 1) calculation by the finite-difference method [10] which coincides with the approximate solution of [11] and numerical solution of [9]; 2) solution with account for capillary forces (We = 0.1) by the method of transfinite interpolation [12].

forces influence only the shape of the surface, whereas condition (1.6) itself for the free surface function is a strongly nonlinear ordinary differential equation of the second order whose solution involves considerable difficulties. Three versions of its realization are possible.

In the case of motion with high velocities or when the surface tension σ is small as compared with K (large Weber numbers $We = \rho u^2 2a/\sigma$), we may neglect capillary forces in the first approximation. The model obtained was solved by various methods: in Lagrange coordinates with the aid of series expansion in powers of time t [5]; by solving numerically an integro-differential equation for the free surface function [9]; by direct finite-difference solution of equations (1.1)-(1.7) [10]. Qualitatively (as regards the shape of the bubble), all the solutions agree well (Fig. 1). At the rear of a rising, originally spherical, bubble an inward depression appears with time which then grows rapidly. The boundary of the free surface remains smooth.

It should be noted that in the calculations of [9] the volume of the bubble remained invariant. With time the bubble boundary approaches the coordinate origin and singularity appears in the coefficients of the equations. Moreover, a situation is possible where the free surface cannot be described by a single-valued function of type $r = R(\theta, t)$. Parametric representation for the function of the boundary makes it possible to avoid these difficulties. The algorithm of the solution of free-surface problems [13] is very much in keeping with the spirit of the method suggested in [9].

Explicit account for capillary forces in Eq. (1.6) in the numerical solution leads to the smoothing of the depression on the back side and does virtually not alter the remaining portion of the boundary (if the curvature radius is large, the value of σK (or K/We) will be small; over portions with a larger curvature the influence of σK is higher; in this case the capillary forces play a dissipative role).

In order to elucidate the actual contribution of capillary forces to deformation processes on a free surface, it is necessary that the curvature-involving term be taken for numerical solution from the "upper time layer," but this greatly complicates the solution algorithm [12]. At large Weber numbers (even at We = 10) solutions coincide with calculations in which capillary forces are not taken into account. However, at smaller We numbers (~ 0.1) there are substantial differences. With the appearance of a depression on the back side in the region of the boundary deflection a wave appears which increases with time (curve 2 in Fig. 1) and then "overturns." The bubble separates into two parts: the upper part rises, while the lower forms an inward rivulet which moves with an increasing velocity. The explanation for such different occurrences of the processes of free surface deformation should be sought in the dispersion properties of the mathematical models used.

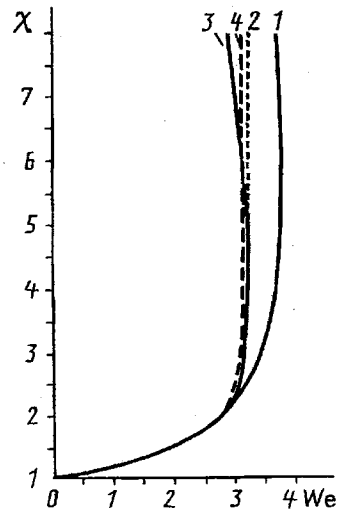

Fig. 2. Degree of bubble deformation as a function of the Weber number according to different methods [19]: 1) two-point theory; 2) linearized two-point theory; 3) virial theory (close to calculations made in [17] and [18]); 4) linearized virial theory.

1.3. Steady rising of a bubble

We can obtain stationary solutions by excluding the gravity-involving term from Eq. (1.2). Physically, this model can be explained as an attempt to take into account the viscous resistance of a bubble balanced out by the Archimedian force. In fact, by integrating Eq. (1.2) (with account for the viscous term [14]) over the bubble surface, we find that the viscosity- and gravity-involving terms disappear. Thus, excluding these quantities from Eq. (1.2), we obtain this approximation. In this case, it is advisable to take into account capillary forces in Eq. (1.6), since after nondimensionalization the problem will have only one independent parameter which usually is taken to be the Weber number. Here the value We = 0 corresponds to a sphere if Eq. (1.6) is fulfilled. It is now apparent that condition (1.6) should be used for determining the shape of the bubble. This greatly complicates numerical solution, since it is necessary to solve the nonlinear curvature operator. When We > 0, the shape of the bubble is close to an ellipsoid [15, 16]. Therefore, in approximate methods of the solution of this problem it was customary to assume that the shape of the bubble was an ellipsoid (see review [3]).

In [17] solutions for the bubble boundary were obtained from an integro-differential equation, and in [18] by a direct finite-difference calculation of the Euler equation. These data and calculations by approximate techniques, for example that of [19], agree well up to We < 2.5 and differ greatly at higher values of We. As We increases, the bubble flattens (see Fig. 2, where χ is the ratio of the horizontal-to-vertical dimension of the bubble). The character of the curve χ(We) is such that when We approaches a certain value ($We_0 \approx 3.3$) the function χ(We) has a vertical tangent. In this case, there is ambiguity of χ(We) in the vicinity of the point We_0. Such a behavior can be interpreted as the bifurcation of the solution with respect of the parameter We with the appearance of an unstable solution, since small deviations ΔWe for the points of the upper branch lead to appreciable changes in the geometric characteristic of the bubble χ. The value of We_0 at which the function χ(We) has a vertical tangent can be adopted to be the critical value which characterizes the stability of a potential flow.

1.4. Dispersion properties of a free surface

The study of the laws governing the propagation of waves over a free surface in their full statement is a very complicated problem even in the simplest case of a plane surface. Some information was obtained for the case where surface deformation occurs with deviation along the normal from equilibrium for waves whose amplitude is much smaller than their length. For the case of the natural oscillations of a spherical incompressible liquid drop

under the influence of capillary forces the Rayleigh solution is used (see [20]). The least possible frequency of oscillations is obtained:

$$\omega_m^2 = 8\sigma/\rho a^3 .$$

Here a is the sphere radius.

Investigation of the dispersion properties of the surface of a bubble or a drop is complicated by the fact that during their motion along the boundary the angle between the direction of the gravity force and the tangent to the surface varies. Nevertheless, the results available for gravity and capillary waves on a plane surface can be applied to waves propagating over the bubble (drop) surface if their length is much smaller than their size. Thus, this offers explanation for the differences in the deformation of a bubble indicated in Sec. 1.2. In fact, if the capillarity effect is neglected, then the dispersion relation for plane waves propagating along the surface has the form $\omega^2 = gk$ (purely gravitational waves [21]). Here, ω is the cyclic frequency and k is the wave vector of the wave. The wavelength is $\lambda = 2\pi/k$, and the speed of wave propagation is $U = \partial\omega/\partial k$ [20]. Substituting the value for ω, we find that the speed of propagation of gravity waves is $U = (g\lambda/2T)^{1/2}/2$. It increases with growth in wavelength. In this case small perturbations originating on the free surface are "stretched" by longer waves (or by the bubble surface itself, which is a wave per se).

The capillary forces in the dispersion relation are taken into account by the term $\omega^2 = gk + \sigma k^3/\rho$. For a short wave we can neglect the influence of the gravity field. Then, $\omega^2 = \sigma k^3/\rho$, and the speed of wave propagation $U = (3\sigma k/2\rho)^{1/2} = (3\pi\sigma/\lambda\rho)^{1/2}$ increases with decrease in wavelength. In this case small perturbations have a high speed of propagation, overcome the longer waves, and strengthen them.

The capillary properties of the free surface of a bubble can be demonstrated if we write the equation for the surface in parametric form [12]. In this case for the functions $R(\xi, t)$, $G(\xi, t)$, and $\tilde{\varphi}(\xi, t)$ ($r = R(\xi, t)$, $\theta = G(\xi, t)$ is the parametric representation of the relation $r = R(\theta, t)$, $\xi \in [0, 1]$) we obtain a system of nonlinear equations not readily amenable to solution:

$$G_\xi R_t - R_\xi G_t = A(\xi, t), \quad R_\xi R_{\xi\xi} + R^2 G_\xi G_{\xi\xi} + R R_\xi G_\xi^2 = B(\xi, t),$$

$$\tilde{\varphi}_t + \frac{1}{J}[(R_k - R) G_t - (\pi\xi - G) R_t]\tilde{\varphi}_\xi = C(\xi, t) -$$

$$- \sigma R (R_{\xi\xi} G_\xi - R_\xi G_{\xi\xi})(R_\xi^2 + R^2 G_\xi^2)^{-3/2}. \tag{1.8}$$

Here the functions $A(\xi, t)$, $B(\xi, t)$, $C(\xi, t)$ designate the terms which do not contain time derivatives and second derivatives with respect to ξ, J is the Jacobian, and $r = R_k$ is the "actual infinity."

Direct elimination first of, say, G_t from the first and third equations of system (1.8) with account for the second equation and then of R_t leads to the following evolutional system of equations:

$$G_\xi \tilde{\varphi}_\xi R_t = \frac{\sigma R_\xi}{R(R_\xi^2 - R^2 G_\xi^2)^{1/2}} R_{\xi\xi} + D(\xi, t),$$

$$- R_\xi \tilde{\varphi}_\xi G_t = \frac{\sigma G_\xi R^2}{(R_\xi^2 + R^2 G_\xi^2)^{1/2}} G_{\xi\xi} + E(\xi, t). \tag{1.9}$$

One equation of system (1.9) is parabolic and the other is antiparabolic, since the set of the factors on which the signs of the terms with R_t, $R_{\xi\xi}$, G_t, $G_{\xi\xi}$ depend is the same, whereas the left-hand sides in Eqs. (1.9) have opposite signs. Thus, the Cauchy problem for system (1.9) is always incorrect.

However, if in Eqs. (1.8) the time derivatives R_t, G_t are excluded so as to drop the terms with R_t and $G_{\xi\xi}$ and with G_t and $R_{\xi\xi}$, we obtain the following system of equations:

$$-\tilde{\varphi}_\xi R_t = \frac{\sigma R}{(R_\xi^2 + R^2 G_\xi^2)^{1/2}} G_{\xi\xi} + P(\xi, t),$$

$$-\tilde{\varphi}_\xi G_t = -\frac{\sigma}{R(R_\xi^2 + R^2 G_\xi^2)^{1/2}} R_{\xi\xi} + Q(\xi, t). \tag{1.10}$$

This system of equations with initial conditions seems to be correct, since it can be reduced to two equations of the type

$$\tilde{\varphi}_\xi^2 R_{tt} + \sigma^2 (R_\xi^2 + R^2 G_\xi^2) R_{\xi\xi\xi\xi} = T(R, G, \tilde{\varphi}), \tag{1.11}$$

whose coefficients are always positive. And this is none other than the equation for the oscillation of a rod which is correct with the initial problem [22]: $R = R_0$, $\partial R/\partial t = R_1$ for $t = 0$.

The dispersion relation for (1.11) (this can be obtained from the full original statement without any assumptions about the displacement of liquid; in particular bending displacements are permissible) has the form

$$-\tilde{\varphi}_\xi^2 \omega^2 + \sigma^2 (R_\xi^2 + R^2 G_\xi^2) k^4 = 0. \tag{1.12}$$

In this case the speed of the propagation of perturbations $U \sim 1/\mathrm{We}\lambda$ is smaller at large Weber numbers and grows with a decrease in wavelength. (There is a similar situation in the problems of the propagation of vibrations in rods and plates. Account for flexural deformations leads to the change in the dispersion relation which has the form of Eq. (1.12)). The appearance of inflection in the free surface (Fig. 1) makes it possible to distinguish waves of several scales on it: long waves corresponding to the upper portion of the bubble, short waves corresponding to the "depression," and even shorter waves corresponding to the region of inflection. Small pertubations propagating over the free surface will first of all influence the deformation in the region of inflection. One should also take into account the effect from $\tilde{\varphi}_\xi(\xi, t) \neq \text{const}$: $U \to \infty$ when $\tilde{\varphi}_\xi \to 0$.

In experiments in liquids with small M values ($\mathrm{M} = g\rho^3\nu^4/\sigma^3$ [23]) the surface of rising bubbles is virtually "scarred with wrinkles." Thus, to get an adequate idea about the character of the deformation of the surface, it is necessary to employ a mathematical model in which capillary forces are taken into account (M = 0 corresponds to an ideal liquid).

Chapter 2. MODEL OF A VISCOUS LIQUID

If a bubble is located in a viscous liquid, the flow is described by Navier-Stokes equations. Despite the viscous resistance of the bubble, the presence of the gravity force makes the process of bubble rise unsteady due to a decrease in the hydrostatic pressure with rise of the bubble and increase in its volume. However, this change in the volume can be small over separate paths of the rise if the bubble is in a state of equilibrium and small compared to the path considered. Usually, in practice such areas are selected far under the free surface, and the degree of the bubble expansion is specially checked. The observation area should be much smaller than the depth of immersion so that the change in the hydrostatic pressure over it is small compared to the pressure within the bubble (estimates made in [3, 24] show that this requirement is not burdensome). Such a quasistationary rise can be simulated by the problem of steady flow around a bubble. This problem was solved exactly in [25, 26]. In this case we have a bubble in equilibrium, and the Archimedian force is balanced by frictional viscosity. This means that over a certain portion of the rise path its volume will not be grossly enlarged. Of course, here the question remains untouched concerning the theoretical accuracy of the approximation the answer to which can be given only by the solution of the unsteady problem of a rising bubble (not necessarily in the three-dimensional case). Indirect confirmation of such a simulation is given by a comparison of experimental data on the speed of the rise of bubbles with calculations for steady flow.

2.1. Statement of the problem

The Navier-Stokes equations describing the motion of a gas cavity in a viscous incompressible liquid have the form

$$\frac{\partial \mathbf{v}}{\partial t} + \mathbf{v}\nabla\mathbf{v} + \nabla(p/\rho + gx_3) = \nu\nabla\mathbf{v}, \tag{2.1}$$

$$\operatorname{div}\mathbf{v} = 0. \tag{2.2}$$

Here $\mathbf{v}(t, \bar{x})$ is the liquid velocity vector at the point with the coordinate $\bar{x}$ at the time t, $p(t, \bar{x})$ is the liquid pressure, and ν is the coefficient of kinematic viscosity.

Let us formulate the boundary conditions. Suppose Σ is the known external boundary of the flow region. Then, the velocity vector $\bar{a}$ $(t, \bar{x})$ is prescribed on it

$$\mathbf{v}|_{\Sigma} = \bar{a}. \tag{2.3}$$

On the free boundary Γ $(F(t, \bar{x}) = 0)$ kinematic and dynamic conditions should be fulfilled

$$\frac{\partial F}{\partial t} + \mathbf{v}\nabla F = 0, \tag{2.4}$$

$$\tau\, T\mathbf{n} = 0, \tag{2.5}$$

$$\mathbf{n}T\mathbf{n} = \sigma K - p_g. \tag{2.6}$$

Here τ, $\mathbf{n}$ are the unit vectors of the external normal and tangent to Γ, and T is the stress tensor $(T_{ij} = -p\delta_{ij} + \rho\nu(\partial v_i/\partial x_j + \partial v_j/\partial x_i))$.

Equations (2.1) express the equilibrium of the forces acting on a liquid particle; Eq. (2.2) is the mass conservation equation; Eq. (2.3), in which $\bar{a}$ is a given function, is usually called the "nonslip condition"; Eq. (2.4) imposing conditions on Γ means that the velocity of liquid particle motion along the normal to Γ coincides with that of the surface displacement in the direction of the normal to Γ; Eq. (2.5) means the absence of friction on the free surface (equality to zero of shear stresses); Eq. (2.6) shows that the difference of normal stresses is equal to the capillary pressure.

Generally speaking, conditions (2.3)-(2.6) do not yet determine the correctly stated problem for Eqs. (2.1) and (2.2) [6]. Additional conditions, i.e., the conditions at infinity for an infinite region, periodicity conditions, and others, are prescribed depending on the specific problem to be solved.

Let us consider the problem of a "steady" rise of a gas cavity in a viscous liquid at rest at infinity. In this case, for $F(t, \bar{x}) = x_3 - f(t, x_1, x_2) = 0$ we have $\partial f/\partial t \to \text{const} = u$ which is called the bubble rise velocity. In the case of steady motion Eqs. (2.1) are simplified and become stationary in the coordinate system "connected with the bubble," i.e., that moving along the direction of the bubble rise with the velocity u (thus we have passed to the problem of flow around a bubble). We will consider axisymmetric solutions. In this case it is convenient to introduce a spherical coordinate system (r, θ, φ) with the origin 0 at the center of mass of the bubble and to pass from the functions of the velocity vector $\mathbf{v}$ and pressure p to the stream function ψ and vorticity ω $(v_r = 1/r^2 \sin\theta \cdot \partial\psi/\partial\theta$, $v_\theta = -1/r \sin\theta \cdot \partial\psi/\partial r)$.

2.2. Dimensional analysis

The problem of a steady rise of a bubble (drop) involves a quantity which is determined by the hydrodynamics of the process, i.e., the rise velocity u. Condition (2.6) incorporates the difference between the

values of pressure constants: within, p_g, and outside, p_∞, the bubble. We will show that the volume of the bubble (drop) is determined by this difference and by the σ value if the media are prescribed. In fact, in the case of equilibrium (e.g., $g = 0$ or $\rho_1 = \rho_2$ for a drop) Eq. (2.6) yields

$$\frac{p_g - p_\infty}{\sigma} = K, \tag{2.7}$$

i.e., the curvature of Γ is constant, and, consequently, the surface is a sphere of radius a. In this case $K = 2/a$, and Eq. (2.7) yields

$$a = \frac{2\sigma}{p_g - p_\infty}. \tag{2.8}$$

Thus, problem (2.1)-(2.6) involves five independent inlet dimensional parameters

$$\rho, \nu, \sigma, g, p_g - p_\infty. \tag{2.9}$$

From the dimensionality theory [27] it follows that the solution depends on two independent dimensionless groups.

Nondimensionalization can be performed by different techniques. Usually, in an experiment one can easily assign the bubble volume V (and, consequently, a certain linear dimension $a = \sqrt[3]{3V/4\pi}$). Moreover, since condition (2.3) incorporates u, it is convenient to take $2a$ and u as the characteristic dimension L and characteristic velocity v. (It should be borne in mind that in Eq. (2.9) two particular parameters will become determinable. In the present case these are g and $p_g - p_\infty$).

Assuming that $r = Lr'$, $\psi = L^2 v\psi'$, $\omega = v/L\omega'$, $R = LR$, and $q = \rho v^2 q'$, where the primed quantities are dimensionless, and substituting them into the motion equations and boundary conditions, we obtain the following parameters: $\mathrm{Re} = vL/\nu$, the Reynolds number, $\mathrm{We} = \rho v^2 L/\sigma$, the Weber number; $\mathrm{Fr} = v^2/gL$, the Froude number; and $Pd = (p_g - p_\infty)L/\sigma$, the dimensionless pressure difference.

Thus, we have four dimensionless groups. According to the dimensional analysis only two groups can be independent. Here, they are taken to be Re and We. The remaining parameters are determinable and should be calculated simultaneously with the flow functions from the assumption of stationarity of flow and constancy of volume (the input data include u and $2a$!). From this it follows, in particular, that with this nondimensionalization technique it is impossible to obtain a solution for a previously specified medium.

Many of experimental and theoretical works also use the Etvesh number, $E = \rho g(2a)^2/\sigma = \mathrm{We}/\mathrm{Fr}$, [28-30, etc.] which coincides with the Bond number, $N_v = u\sqrt[4]{(\rho/g\sigma)} = \sqrt[4]{(\mathrm{WeFr})}$, $N_b = \sqrt{E}$ [31], as well as the Morton number, $\mathrm{M} = g\rho^3\nu^4/\sigma^3 = \mathrm{We}^3/\mathrm{Re}^4\mathrm{Fr}$ [32-34, etc.]. The group of physical quantities M was obtained for the first time by Kapitsa [35] when he investigated thin films flowing down a vertical wall. In the literature this group is denoted by $Fi = 1/\mathrm{M}$, which is the film number. In publications devoted to the problems of the rise of bubbles the number $\mathrm{M} = g\mu^4/\rho\sigma^3$ is used. Moore [36] mistakenly indicated that this dimensionless group was introduced for the first time in [37]. It was Schmidt [38] who first introduced the number M. The quantity M was called the Morton number beginning about 1970. This parameter is very convenient, since it involves only dimensional physical quantities characterizing the liquid, and does not incorporate the characteristic dimension of a bubble (drop) and the rise velocity. More to the point, $\mathrm{M} = \mathrm{Ar}^{-2}$, where Ar is the well-known modified Archimedes number [39] when the "capillary Laplace constant" is taken as the characteristic length, $\delta_\sigma = \sqrt{\sigma/\rho g}$.

The resistance coefficient Cd is usually defined as the ratio of the resistance force to dynamic pressure, and in the given case, since for a "steady" rise of a bubble the resistance force is equal to the Archimedian force, we have $Cd = \rho Vg/(1/2\rho v^2 \pi a^2) = 4/3\mathrm{Fr}$. (For a gas bubble $Cd = (1\ \rho_1/\rho_2)\cdot 4/3\mathrm{Fr}$). Thus, the determination of Fr is equivalent to the computation of the resistance coefficient of a bubble.

The representation of results and the construction of the charts of flow modes in coordinates with the parameters Re, We, E, and N_v turn out to be unsatisfactory, since they incorporate the characteristic dimension and rise velocity which, as a matter of fact, are quantities to be determined. The parameters most convenient for the purpose are $R_\sigma = a/\sqrt{\sigma/\rho g}$ and $R_\nu = a/\sqrt[3]{(\nu^2/g)}$ [40, 41]. Since $(R_\sigma/R_\nu)^6 = \mathrm{M}$, the data for each rise medium

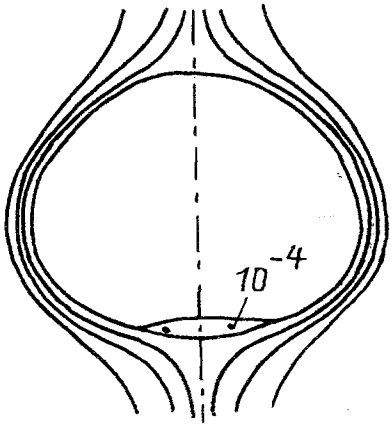

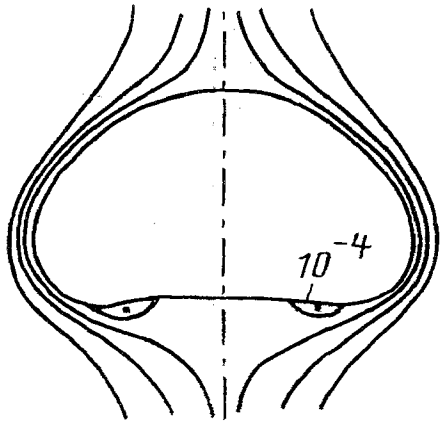

Fig. 3. Shape of a bubble and flow structure for media with large M values: M > 0.004 (Re = 3, We = 8).

Fig. 4. Flow separation in media with "intermediate" M values: 10^{-4} < M < 0.004 (Re = 12, We = 7.66).

are represented in the diagram with the coordinates R_σ and R_ν on a certain straight line whose slope is determined by the value of M. Having constructed the isolines of the Froude number Fr (or Cd), it is possible to very easily find the rise velocity for a bubble of a given size and focus our attention on the special features of flow for a particular liquid. The parameters are interrelated as follows:

$$R_\sigma = (\mathrm{We}/4\mathrm{Fr})^{1/2}, \quad R_\nu = (\mathrm{Re}^2/8\mathrm{Fr})^{1/3}.$$

The quantity $\delta_\sigma = \sqrt{\sigma/\rho g}$ entering into the definition of R_σ is called the capillary constant of the liquid. It characterizes the balance of the forces of gravity and surface tension and is an important characteristic for the processes of the rise of bubbles and drops.

If the value $L = \rho\nu^2/\sigma$ is taken as the characteristic size L and $v = \sigma/\rho\nu$ as the characteristic velocity and nondimensionalization is made in its usual manner, then in Eqs. (2.1)-(2.6) instead of Re, We, Fr, and Pd we will have Re ≡ 1, We ≡ 1, Fr = 1/M, and $Pd = 2\sqrt{\mathrm{M}}/R_\sigma$. At infinity the liquid moves at a constant velocity $u_* = u/v = u/(\sigma/\rho\nu)$.Thus, the motion equations and boundary conditions contain three dimensionless groups: M, R_σ, and u_* (in Pd allowance is made for the fact that in the case of equilibrium Eq. (2.6) yields $2\sigma/a = \rho_g - \rho_\infty$). Here R_σ prescribes the size of a bubble, M depends only on the physical constants of the liquid, g characterizes the rise medium, and u_* is the determined quantity. In [42] an algorithm was constructed to generate the solution of the problem for determining u_*.

2.3. Results of calculations

In [25, 26] an algorithm is suggested for direct finite-difference solution of the Navier-Stokes equations with simultaneous determination of the bubble boundary, and data are given on the laws governing the free surface deformation.

Ryskin and Leal [43] cite an example of the use of the adaptive mesh method to calculate flow around a bubble. The solutions obtained correlate well.

From condition (2.6) it follows that, for any Re values, We = 0 corresponds to the spherical bubble (drop). At fixed Re and increasing We numbers the bubble flattens vertically. Moreover, at small values of Re a depression appears at its rear in which a stagnant zone is formed at a certain We_0 value (Fig. 3). At higher Re values a vortex wake (separation) appears on the edges of the plane back side (Fig. 4). When Re ≥ 40, the vortex exists even with the convex shape of the bubble. When We > We_0, there is an extensive stagnant zone behind the bubble. The intensity of liquid motion in it is not high. The foregoing is illustrated in Fig. 5 which presents the calculated

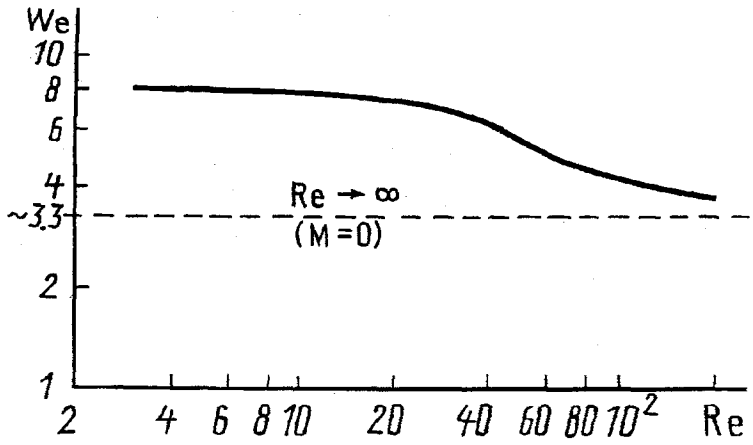

Fig. 5. The values of Re and We pointing to the appearance of an eddy wake behind the bubble.

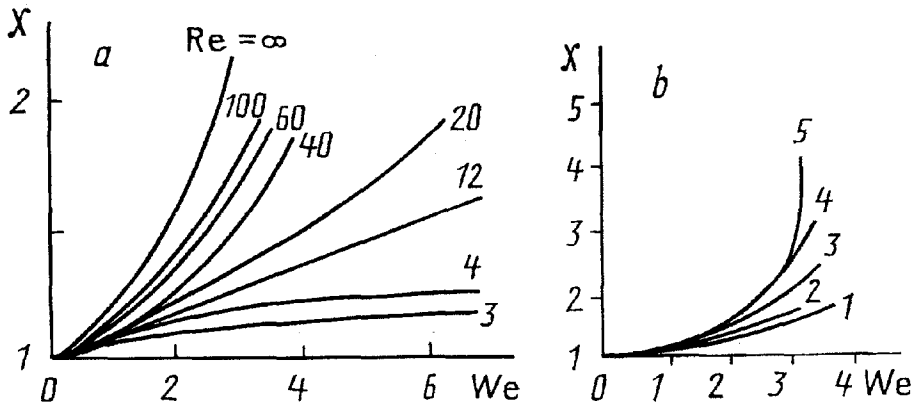

Fig. 6. Degree of bubble deformation as a function of the Weber number for different Reynolds numbers (a) and media with $M = 10^{-5}$ and $1.8 \cdot 10^{-7}$ (b): 1,2) calculations in [26]; 3, 4) calculations by the approximate model of [14]; 5) M = 0.

dependence of the Weber and Reynolds numbers, indicating the appearance of the stagnant zone. As the Reynolds number increases, We_0 decreases. Thus, the last stationary solution at Re = 200 was obtained for We = 3.8. The flow near the bubble is separationless and the stream function on the back side is equal to $\sim -10^{-4}$. This means (taking into account the solution at smaller Reynolds numbers) that flow separation is about to happen "soon" with the formation of a stagnant zone behind the bubble. In this case the value of χ is equal to about 1.8. The dashes give the line corresponding to $We_0 = 3.3$ (see Sec. 1.3, the model of an ideal liquid).

Figure 6a presents graphs of χ(We) calculated for the front part of a bubble at different Re values. At small Reynolds numbers the curves χ(We) approach certain constants. This means that deformation occurs at the rear as the depression is enlarged. At large Re numbers the functions χ(We) tend to approach vertical straight lines, and as Re rises they approach the χ(We) value of the ideal liquid (Re → ∞). This means that upon attainment of certain We_k values the solutions become unstable: small additions ΔWe lead to large changes in the bubble geometry, and calculation becomes impossible. The behavior of the functions χ(We) for different Re values, as well as the closeness of the values of We_0, which were obtained with the help of the model of ideal (≈ 3.3) and viscous (≈ 3.8) liquids and which point to the presence of instability in the solution, indicate that the value $We_0 \approx 3.3$ corresponding to the lower branch of the function χ(We) in the ideal liquid model (in the ellipsoidal bubble approximation according to [19] We ≈ 3.271) seems to be the critical value at which the rise proceeds stably. The data of Fig. 6a can be recalculated for the prescribed media by constructing graphs of χ(We) for constant values of

M. These graphs have the same form. In Fig. 6b the results of calculations from [26] for media with $M = 10^5$ and $1.8 \cdot 10^{-7}$ are compared with the data of [14] in which the viscosity-containing terms are taken into account in the dynamic condition within the framework of the ideal liquid model. As M falls, the functions $\chi(We)$ for the given M approach the graph of an ideal liquid (M = 0).

Taking into consideration the character of the functions $\chi(We)$, we may assert that in media with small M values, starting with certain values of We (≈ 3), a large scatter will be observed in the experimental values of χ and, consequently, in the rise velocity. This is confirmed by the data of [44] for the critical Re number at which the rise is still straight, varying for water from 200 to 600. In doubly distilled water the critical value is $\chi \approx 1.75$ [45] (which corresponds to $We \approx 2.6$). In a pure low viscosity liquid such as water $We_k \approx 2.52$, whereas at large We numbers the bubble begins to "levitate."

Different reasons are possible for the appearance of instability: purely hydrodynamic reasons associated with the motion of gas in a bubble, the presence of surfactants and admixtures, and the degree of perturbation in the system. As a rule, the latter items are specified and checked in the literature and experiments: the selection of a medium for experiments, the means of producing bubbles, the selection of the area for observation, and the method of data acquisition - all this can substantially influence the quality of the experimental data obtained. Therefore, to exclude in practice the effect of surfactans in water, the latter should be distilled three times and the corresponding chemical treatment of the apparatus should be made. As regards the second item, it is generally accepted that the effect of gas motion in the bubble on the hydrodynamics of its rise can be neglected [3]. However, a precise answer can be found only through the corresponding theoretical investigation.

2.4. Flow separation on a bubble

A numerical solution of the problem offers an excellent possibility to elucidate the quantitative and qualitative characteristics of the most important phenomenon of hydromechanics, i.e., separation of flow from a surface immersed in it. It is presumed that separation from a solid surface occurs due to the clinging of a viscous fluid and the formation of vorticity on it [24]. In the case of a bubble, the condition of the absence of shear stresses and friction is assigned on the boundary. Thus, we eliminate one of the most important reasons which causes flow separation, and the last reason remains, i.e., the presence of a boundary layer in which the liquid velocity changes from unity on the outer side to a certain value on the bubble boundary. This means that the main role in the mechanism of flow separation is played by the adverse pressure gradient on the rear which leads to the retardation of the flow.

At small Reynolds numbers ($Re < 5$) the generalized pressure function on the surface of a spherical bubble decreases monotonically in motion from the forward to the backward stagnation point [46]. In this case the flow is separationless. As the surface undergoes deformation, the pressure on the back side rises, a segment with an adverse gradient appears, and at a certain value of We_0 (Fig. 5) a vortex is formed. At large Re numbers a region with an adverse pressure gradient already appeares on the sphere, and the flow can separate as directly at the rear of the bubble as on the edges of its flattened back side [47]. In the region of the vortex wake the pressure on the boundary is virtually constant, whereas the liquid velocity is very small (Fig. 7).

The appearance of the vortex wake downstream of the bubble obliterates the individual features associated with the bubble shape and leads to the "self-similarity" of the rise velocity with respect to one of the hydrodynamic parameters. In liquids with high M values we have a bubble and an attached vortex, both close to a sphere. The experimental data of work [30] agree well with the calculations in [26]. The geometric characteristics of the bubble and wake, and the flow separation angle, depend on the same parameter, i.e., the Reynolds number. Only when $Re > 110$ does the wake behind the bubble open and become unstable.

In media with small M values we have a flattened ellipsoidal bubble with a long wake ($Re > 60$). The pressure on the bubble surface in the region of the wake is practically constant. At the front of the bubble, since the boundary layer on it is $\sim Re^{-1}$, the pressure can be found from the Bernoulli integral [48], since the bubble resistance is independent of viscosity. Irrespective of the liquid, large bubbles on the surface have the shape of a

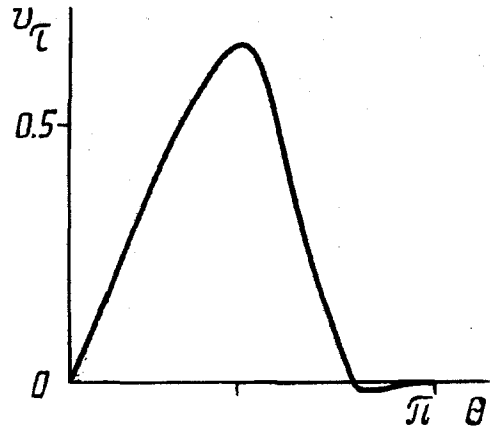

Fig. 7. Liquid motion velocity on the surface of a bubble: Re = 12, We = 7.9.

spherical cup with a vortex at the rear. In this case the quantity 2Fr tends to unity with increase in bubble volume [49].

For very small M values, stationary solutions were obtained for We < 4 (large Re numbers). At higher We values, in the iterations of the calculations of the boundary the bubble alternately flattens and expands again. Its shape is close to a flattened ellipsoid with $\chi \simeq 1.8$. The value of the stream function on the bubble rear is equal to about -10^{-4}. Taking into account solutions at smaller Re values, this signifies "impending" separation. However, here the steady regime was not attained despite large expenditures of computation time. Experiments in solutions of glycerin [47] and the data of [44] for media with $1.6 \cdot 10^{-10} \leq M \leq 5.85 \cdot 10^{-7}$ indicate that a wake is present and that the rise occurs along a spiral. Thus, we may conclude that in low-viscosity liquids (with small values of M) the formation of a vortex leads to instability in the linear rise of the bubble.

Finally, since we consider the "stationary" rise of a bubble, we must analyze Fig. 5 in which We_0 is plotted as a function of Re. Everywhere below the curve there is a rising bubble without a vortex and above the curve there is a wake. The character of the curve $We_0(Re)$ is such that at relatively small Re values ($3 \leq Re < 20$, or in rather viscous media with M > 0.001) for $We \geq \approx 8$ there is a vortex wake supplementing the bubble almost up to a sphere. At rather large Re values (> 100 or in media with $M < \approx 10^{-6}$) when We ≥ 3.5-4 a long wake appears behind a flattened ellipsoidal bubble which in liquids with $M < \approx 10^{-7}$ leads to the loss of the stability of the linear rise. In media with $10^{-6} < M < 10^{-3}$, corresponding in Fig. 5 to the transitional region, the value of We_0 depends substantially on the liquid and on the structure of flow.

When Re < 3 (in liquids with M > 10) no vortex wake was revealed. The deformation of the surface (even a very small one) led, starting from a certain We value (corresponding approximately to $R_0 \simeq 3$), to instability in the calculations of the flow field (Re = 1, We ≈ 2; Re = 0.1; We ≈ 0.1).

2.5. Data correlation, a chart of flow regimes

When numerical data were discussed and compared with the results of experiments, difficulties arose due to the use of different sets of parameters to describe rising bubbles. Traditionally, experimental data are expressed as a dependence of the rise velocity of a bubble u on its size a. In this regard, Fig. 8 from work [50] is exemplary. Large bubbles in different liquids rise with the same velocity, with the law of the rise being formulated with good accuracy as $Fr = u^2/ga \simeq 1$ (see also [49]). The bubble has the shape of a spherical cup with a large vortex zone behind it (supplementing it almost up to a sphere). With smaller sizes of the bubble the curves for different liquids intersect and it is difficult to perform any comparative analysis. Harper [34] distinguishes between two types of behavior of these curves: monotonically growing with an increase in the bubble volume, and those having a local maximum. He suggested using M as the parameter responsible for such a division. In [30] it is indicated that a liquid with M = 0.004 can be regarded as a separating one.

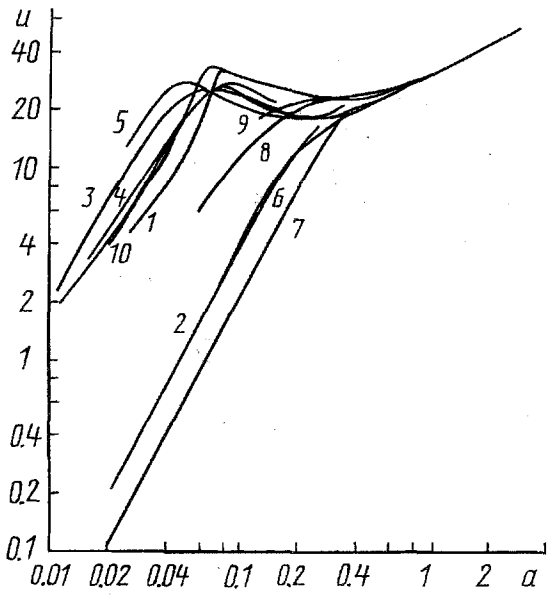

Fig. 8. Bubble rise velocity (cm/sec) in various media as a function of the equivalent radius [50]: 1) water, $M = 1.8 \cdot 10^{-10}$; 2) mineral oil, $M = 1.45 \cdot 10^{-2}$; 3) varsol, $M = 4.30 \cdot 10^{-10}$; 4) turpentine, $M = 2.41 \times 10^{-9}$; 5) methyl alcohol, $M = 0.89 \cdot 10^{-10}$; 6) a 62% solution of syrup in water, $M = 1.55 \cdot 10^{-4}$; 7) a 68% solution of syrup in water, $M = 2.12 \cdot 10^{-3}$; 8) a 56% solution of glycerin in water, $M = 1.76 \cdot 10^{-7}$; 9) a 42% solution of glycerin in water, $M = 4.18 \cdot 10^{-8}$; 10) a 13% solution of glycerin in water, $M = 1.17 \cdot 10^{-8}$. u, cm/sec; a, cm.

The segregation of media by the parameter M turns out to be natural if the dimensionless groups $R_\sigma = a/(\sigma/\rho g)^{1/2}$ and $R_\nu = a/(\nu^2/g)^{1/3}$ are used as coordinates for constructing a chart of modes. Since $M = (R_\sigma/R_\nu)^6$, the data for each medium are expressed on a certain straight line whose slope is dictated by M. In this case all of the media are ordered in conformity with the quantity M, and a comparative analysis of the specific features in the rise of bubbles in a given medium becomes simple.

In Fig. 9 the line inclined at an angle of 45° to the R_σ axis corresponds to the medium with M = 0.004. First of all, we note the good coincidence between the experimental and calculated data for the Froude number. Since R_σ and R_ν are independent of the rise velocity u, the value of Fr here provides complete information on u, and using the isolines Fr = const one can easily assess the dependence of u on the bubble size a for specific media. There are two types of isolines which can be separated by a straight line representing a medium contacting a certain line Fr = const for the first time. For all of the media below this line, the graph of the rise velocity rises monotonically with growth in the volume, since their straight lines intersect the isolines with increasing constants on them. For media above this line the graph of the rise velocity has a local maximum. Here, as a separating medium we can take with a good accuracy a liquid with M = 0.004 (perhaps, with a slightly smaller value $M \simeq 0.001$, which is insignificant as a whole, as it is preferable to isolate a certain class of media for which the graph of the rise velocity has an inflection).

In Fig. 9 the dash-dotted lines represent zones I-V with characteristic types of flows indicated schematically. In the region of spherical bubbles (I) the isolines Fr = const are linear and parallel to the axis R_σ: the flow is determined by one dimensionless parameter which is usually taken to be the Reynolds number (the capillary forces are large, the surface is a sphere, and everything is dictated by viscous flow).

For media with large M values there is also a region of R_σ numbers where the isolines have the same character (region IV). In this case the bubble and the wake form almost a sphere. Calculations agree well with the data of [30].

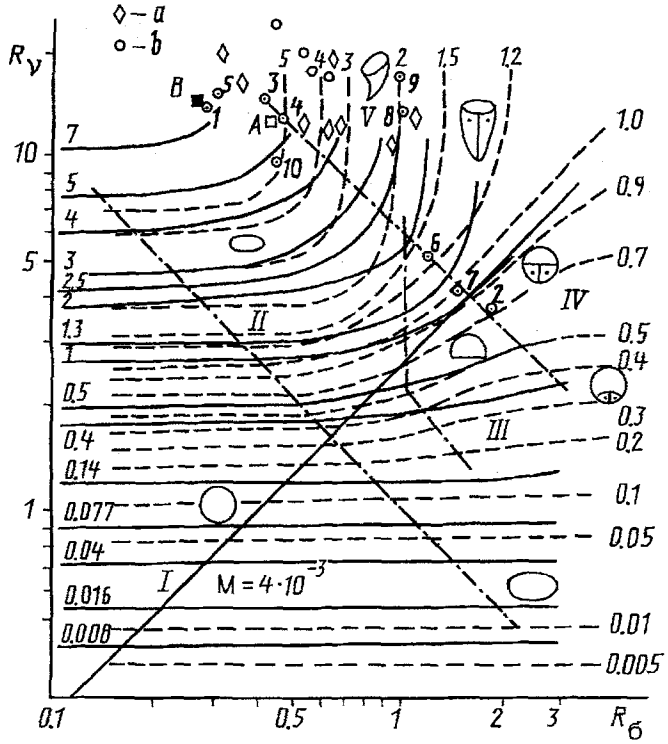

Fig. 9. Chart of the flow modes of a rising bubble and the isolines of the Froude numbers [47]: solid lines, calculations by P. K. Volkov; dashed lines, experiments of various authors; a) data of [44]; b) [47]; points 1-10 correspond to designations 1-10 in Fig. 8.

In media with small M values, the isolines approach straight lines parallel to R_ν (region V). The flow is governed by one parameter independent of viscosity. Here, downstream of the flattened bubble there is a stagnant zone with a practically constant pressure on the boundary, so that the bubble resistance is determined by the degree of flattening (parameter dependent on σ) and by the presence of separation and depends little on ν. This is confirmed by the data of [51, 52] where formulas were obtained for the rise velocity which do not involve ν and which describe the region behind the local maximum.

The upper dash-dotted line indicates the apparance of a vortex wake behind a bubble. This line passes near the points of contact with the straight lines representing a medium (for small M values) with the isolines Fr = const. Thus, the presence of a local maximum in the dependence of the rise velocity on the bubble size can be explained by the appearance of a vortex behind the bubble and by the transition from laminar to separating flow. Points 2, 6, and 7 in Fig. 9 indicate the positions of local maxima in the bubble rise velocity or inflection points from [50], confirming the calculated data. Points 1, 3-5, 8-10 correspond to local maxima in the velocity graph for media with small M values.

In the upper portion of region II stationary solutions are obtained only up to the straight line. Thus, calculations at Re = 200 could not proceed further than We = 3.8 (A in Fig. 9). (The quantity B in Fig. 9 indicates the last stationary solution at Re = 200 obtained from the model of a drop when the inner and outer medium density ratio is equal to 0.1. In this case we can speak of the rise of a vapor bubble. It was also not possible to proceed further. Vibrations appeared in the flow, and stationary solutions were not obtained). Thus, the calculational data indicate that, when We > 3.8, instability appears in the flow before the origination of a vortex wake. This is confirmed by experiments: a and b in Fig. 9 present the experimental data of [44, 47] pointing to the helical rise of bubbles in various liquids. Thus, the instability of flow is caused by the appearance of a vortex at the rear. In low-viscosity media (with small M values) this leads to the rise along a helical line, and then to the retardation of the bubble and to the appearance of local maximum in the rise velocity graph. In media with higher M values the rise is linear with a long wake.

Analysis of experimental data (see [3] and the literature cited there) in terms of the variable $R_\sigma = a/\delta_\sigma$, where δ_σ is the capillary constant of liquid, shows that as a rule the bubble ceases to levitate at $R_\sigma \simeq 1$. For bubbles exceeding in size the capillary constant ($R_\sigma > 1$, the rise is again linear. Comparison with the data of [50] shows that the values of a at which $R_\sigma \simeq 1$ approximately correspond to the local minimum in the dependence of the rise velocity on a for media with small M values. Thus, the local maximum and minimum in the rise velocity graph point rather accurately to the region of unsteady nonlinear rise.

Taking into account the data obtained from the models of an ideal and a viscous liquids, it is possible to calculate the rise of the bubbles in media with small M values by solving Euler equations for We < 3.3. In this case the liquid flow is separationless. At higher We numbers there is separation in liquids with different M values, and a description of the process by the ideal liquid model should take this into account. For this purpose one can use the model of [53], i.e., the flow is potential everywhere outside a certain region behind the bubble where the pressure is assumed to be constant. (The data of calculations by Navier-Stokes equations indicate that this method works well in the wake region). The line separating these regions can be found in the same way as the shape of the bubble [10] or as the line of separation from a solid surface in the model of [53, 54]. Such a statement makes it possible to obtain the resistance coefficient within the framework of the ideal liquid model.

Chapter 3. ALLOWANCE FOR THE MOTION OF THE BUBBLE MEDIUM. RISE OF DROPS

3.1. Statement of the problem

As a rule, when one models bubbles rising in liquid, it is assumed for the simplification of the problem that the medium within the bubble is at rest, and to describe the state of such a medium it is quite sufficient to have one constant, viz. the thermodynamic gas pressure in a bubble p_g. In the case of the rise of gas or air bubbles in a heavy liquid this is quite justifiable, since the ratio of the densities and viscosities of the gas and liquid is $<< 1$, and, consequently, the medium in the bubble is light, so that the friction of the gas against the liquid on the bubble boundary is small and does not exert a substantial effect on the bubble rise. This assumption is confirmed by numerous experiments. However, for vapor bubbles, for example in freons, the density ratio is already of the order of 0.1, and calculations using the model of a bubble are no longer satisfactory.

For the problems of quasisteady rise the simplest way for taking into account the motion of the medium in a bubble is to assume that there is a viscous incompressible liquid within the bubble (a drop of another liquid) with the density ρ_1 and kinematic viscosity ν_1 (ρ_2 and ν_2 are the parameters of the external medium). Then, when $\rho_1 = \rho_2$, the drop is in equilibrium; when $\rho_1 < \rho_2$, it rises, but when $\rho_1 > \rho_2$, it sinks. In any case, one can expect the appearance of steady motion, because the Archimedes force of the drop and the resistance force to the liquid around it act in opposite directions. Since the volume of the drop remains invariant because of the liquid incompressibility (and, consequently, the Archimedes force is constant), there may come an instant when the resistance force becomes the same as the buoyancy force. If in this case the shape of the drop and flow pattern do not change substantially, we may say that there occurs a steady rise (immersion), with the velocity u governed by the hydrodynamics of the process.

The equations of motion describing the axisymmetric steady viscous incompressible liquid flow around a bubble are supplemented with the Navier-Stokes equations for the interior of the bubble. The boundary conditions in terms of the stream function ψ - vortex ω in a spherical coordinate system are: on the droplet surface Γ ($r = R(\theta)$, $\theta \in [0, \pi]$): no-flow condition

$$\psi_i(r, \theta) = 0 \ (i = 1, 2), \tag{3.1}$$

no-slip condition (the equality of velocities tangent to Γ)

$$\frac{R'}{R^2}\psi_{1\theta} - \psi_{1r} = \frac{R'}{R^2}\psi_{2\theta} - \psi_{2r}, \tag{3.1}$$

equality of shear stresses

$$\rho_1 \nu_1 \left(\omega_1 + \frac{R^2 + 2R'^2 - RR''}{R^2 + R'^2} \frac{\psi_{1r}}{R^2 \sin\theta} \right) =$$

$$= \rho_2 \nu_2 \left(\omega_2 + \frac{R^2 + 2R'^2 - RR''}{R^2 + R'^2} \frac{\psi_{2r}}{R^2 \sin\theta} \right), \tag{3.3}$$

equality between the difference of normal stresses and capillary pressure

$$-p_1 + 2\rho_1 \nu_1 \left[\frac{\psi_{1\theta r} - \psi_{1\theta}/R - R'\psi_{1rr}}{R^2 \sin\theta} + \frac{R'}{R}\omega_1 \right] =$$

$$= -p_2 + 2\rho_2 \nu_2 \left[\frac{\psi_{2\theta r} - \psi_{2\theta}/R - R'\psi_{2rr}}{R^2 \sin\theta} + \frac{R'}{R}\omega_2 \right] - \sigma K + p_g - p_\infty . \tag{3.4}$$

Here σ is the surface tension coefficient on the interface between two media; ρ_1 and ρ_2 is the pressure on Γ from the inside and the outside of the drop, respectively; $p_1 = q_1 - \rho_1 gR\cos\theta + p_g$, $p_2 = q_2 - \rho_2 gR\cos\theta + p_\infty$; q_1, q_2 are the generalized pressures; $p_g = p_1$ $(r = 0, \theta)$, p_∞ is the pressure on the outer edge of the flow region at the "level of the drop" $(\theta = \pi/2)$.

On the outer edge of the flow region the liquid has the velocity u

$$\psi_2(r, \theta) \sim -\frac{u}{2} r^2 \sin^2\theta , \tag{3.5}$$

$$\omega_2(r, \theta) \sim 0 . \tag{3.6}$$

On the symmetry axis $(\theta = 0, \pi)$

$$\psi_i(r, \theta) = \omega_i(r, \theta) = 0 \ (i = 1, 2) . \tag{3.7}$$

Thus, we must find the functions ψ_1 and ω_1 determined within the drop, ψ_2 and ω_2 determined outside it, and the function of the surface $R(\theta)$. The correctness of the problem of a liquid drop immersed in a steady viscous flow of another liquid for the case of an infinite region was investigated in [55]. It has been proved that for certain values of the input parameters the solution exists and that it is a unique one.

3.2. Dimensional analysis

Since the drop differs from the bubble by the fact that the medium motion within the bubble satisfies the Navier-Stokes equations, the initial problem involves seven independent input dimensional parameters

$$\rho_1, \nu_1, \rho_2, \nu_2, \sigma, g, p_g - p_\infty . \tag{3.8}$$

From the dimensionality theory [27] it follows that the solution depends on four independent dimensionless groups. In the adopted nondimensionalization technique (Sec. 2.2) these are: $\rho = \rho_1/\rho_2$, density ratio; $\mathrm{Re}_1 = vL/\nu_1$, Reynolds number of a drop; $\mathrm{Re}_2 = vL/\nu_2$, Reynolds number of external flow; We Fr, *Pd*.

According to the dimensional analysis, only four quantities can be independent. Here, we take these to be ρ_1/ρ_2, Re_1, Re_2, and We. The remaining quantities are determined ones and should be calculated simultaneously with the stream functions from the assumption of stationarity of the flow and constancy of the volume (the input quantities also incorporate u and $2a$). From this it follows, in particular, that with this nondimensionalization

technique one cannot obtain a solution for prescribed media. Thus, acquisition of information concerning the processes of rise in specific media requires of parametric calculations and interpretation of the results.

Just as in the case of a bubble, the representation and correlation of results can be conveniently made in the coordinates R_σ and R_ν calculated in terms of the rise medium parameters (Sec. 2.2). In this case the data for each liquid are located on a certain straight line whose slope depends on M, so that direct comparison of diagrams for the drop and bubble is possible. The change in Re_1 at a fixed Re_2 leads to deviations in the values of Fr, from which we can judge the degree of influence of the liquid of the drop on the rise velocity. The increased number of independent dimensionless parameters does not allow one to efficiently analyze the laws governing the rise on one diagram as in the case of a bubble. In this case it is convenient to use the coordinates R_σ, and R_ν to express the lines of constant Reynolds numbers, having denoted on them the values of Fr and the characteristic types of flows. This will allow one, by employing a direct superposition of diagrams for a bubble and a drop, to elucidate the degree of influence of the drop medium on its rise.

The use of the quantities that depend on the physical properties of the rise medium, i.e.,

$$L = \rho_2 \nu_2^2/\sigma, \quad v = \sigma/\rho_2 \nu_2,$$

as the characteristic dimension L and velocity v permits one to obtain, instead of Re_1, Re_2, We, Fr, and Pd, the parameters ν_2/ν_1, 1, 1, M_2^{-1}, $2\sqrt{\mathrm{M}_2}/R_\sigma$, where $R_\sigma = a/\delta_\sigma$, $\delta_\sigma = \sqrt{\sigma/\rho_2 g}$ is the capillary constant of the external liquid; $\mathrm{M}_2 = g\nu_2^4\rho_2^3/\sigma^3$ is the parameter M of the external liquid. The quantity to be determined is $u_* = u/v = u/(\sigma/\rho_2\nu_2)$.

Thus, the motion equations and boundary conditions incorporate dimensionless groups ρ_1/ρ_2, , ν_2/ν_1, M_2, R_σ, and u_*. The first four that depend only on the physical properties of the surrounding medium and drop medium and also on the drop size a are independent, whereas the fifth group, the dimensionless rise velocity, is a determined quantity. An algorithm has been constructed making it possible to obtain the flow functions and the quantity u_* for the given media and size of the drop [56].

3.3. Spherical drop

The first calculations of complete Navier-Stokes equations were made by Rivkind with co-authors (see [4]). The constructed algorithms solved the problem of flow around a drop at a given Froude number. This corresponds to the determination of flow structure at a given free stream velocity u, and, consequently, the solution complies with the problem of drop rise only when u is assumed to be the rise velocity. The flow patterns obtained agree qualitatively with the calculations simulating a steady rise of a drop [57].

The presence of four independent parameters prevents one from carrying out a full investigation of the problem of drop rise; therefore, here we shall limit ourselves to the solutions at $\rho = 0.1$ for two reasons. First, at large Re_1 values there should be a good fit with a bubble. Second, they are also important in their own right since they model the rise of vapor bubbles (for example, in freons, cryogenic liquids at large specific pressures).

The effect of the motion of the drop medium can be simply traced for a spherical drop: We = 0, and condition (3.4) is fulfilled by selecting the difference of pressures $p_g - p_\infty$ (at a given a the boundary should be in equilibrium). Having fixed Re_2, it only remains to solve hydrodynamic problems for different Re_1 values in a given region. The resistance coefficient Cd for a steadily rising drop is calculated from the formula $Cd = (1 - \rho_1/\rho_2)8/3\mathrm{Fr}$ ($\mathrm{Fr} = u^2/ga$). From Table 1 it follows that at $\mathrm{Re}_1 = 60$ the "bubble approximation" works out rather well, and at $\mathrm{Re}_1 = 0.4$, the "approximation of a solid sphere." At small Re_2 values, solutions which are independent of Re_1 are obtained.

The values of Cd at $\mathrm{Re}_1 = 0.4$ are smaller than for a solid sphere [24, 58] by less than 9% for $\mathrm{Re}_2 < 100$. (In experiments, Cd for solid bodies is obtained by the method of immersion of the spheres in liquid under gravity. However, much as we like the idea, we are unable to numerically establish the limiting transition to a solid sphere accurately, since the boundary conditions at the interface of the media differ from the no-slip conditions on the wall. In its form condition (3.3) strongly resembles the familiar dependence for a vortex on a solid wall, i.e., the so-called Thoma condition [59]. It is precisely this fact that seems to be responsible for the

TABLE 1. Resistance Coefficient of a Drop $Cd = (1-\rho_1/\rho_2)\cdot 8/3\mathrm{Fr}$ (Sphere)

Re_2	Re_1					Bubble		Solid sphere [58]
	0.4	20	40	60	100	calculation	data of [60]	
0.1	238	-	-	236	-	160.5	161.6	240
1	25.2	-	-	24.12	-	16.8	17.6	26
12	3.58	-	2.5	-	2.47	2.2	2.2	3.9
40	1.78	-	1	0.93	-	0.8	0.83	1.9
60	1.5	-	-	0.71	-	0.66	0.6	1.6
100	1.28	0.67	-	0.52	-	0.48	0.4	1.2
200	1.13	0.65	-	-	-	0.32	0.2	0.82

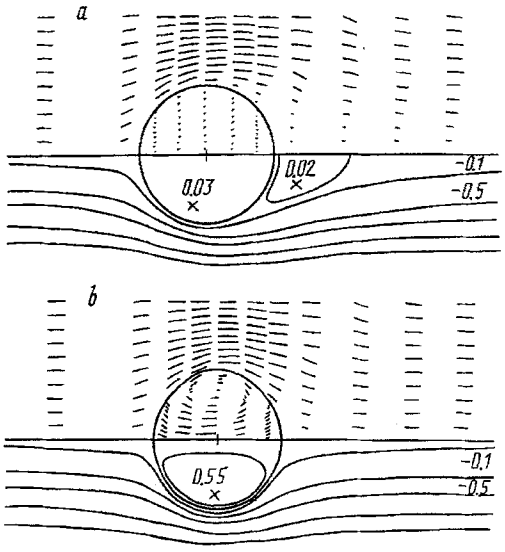

Fig. 10. Pattern of flow near a rising drop: solid curves, isolines of the stream function; dashed lines, velocity vector field; a) $\rho_1/\rho_2 = 0.1$, $Re_1 = 0.4$, $Re_2 = 200$, $We = 0.45$, $M = 2.9\cdot 10^{-11}$, $M_{dr} = 0.004$, $Fr = 2.1$; b) $\rho_1/\rho_2 = 0.1$, $Re_1 = 60$, $Re_2 = 100$, $We = 0.88$, $M = 3.4\cdot 10^{-9}$, $M_{dr} = 10^{-12}$, $Fr = 4.1$, $R_\sigma = 0.33$, $R_\nu = 8.46$.

good coincidence of results in the parametric domain up to the appearance of secondary flows behind the drop.) The external flow is nonseparating, but at $Re_2 = 100$, 200 we already have, behind the sphere, a region of secondary flow which does not close directly on the drop (Fig. 10a). Within the drop and in the wake region there are vortical motions in one direction whose intensity is small. The source of these rotations is the external flow. The internal vortex originates at the expense of friction on the interface between the media, and the external vortex appears due to the retardation of a portion of liquid behind the drop. The absence in the flow pattern of the separating line originating on the sphere surface is associated with the necessity of joining two vortical motions (inside and outside of the drop) in one direction. For the boundary line of the secondary flow to originate at the drop surface, a third "buffer" vortex between these two should appear, which rotates in the opposite direction. Such a flow structure is possible at rather intense vortical motion behind the drop (or in the case of a low-viscosity and "light" medium in the drop), which can induce flow on a portion of the boundary and thus organize a new reverse flow within the drop. Such processes actually occur with an increase in We. At $We = 0.46$ ($Re_1 = 0.4$, $Re_2 = 200$, a slightly deformed sphere) in the iterations of calculations by fictitious time, as soon as a new "buffer" vortex has been generated within a drop, the external vortex starts to depart and a new vortex is formed which borders directly on the surface; it develops up to the size at which the flow again becomes steady (B in Fig. 11) or the process will become unsteady.

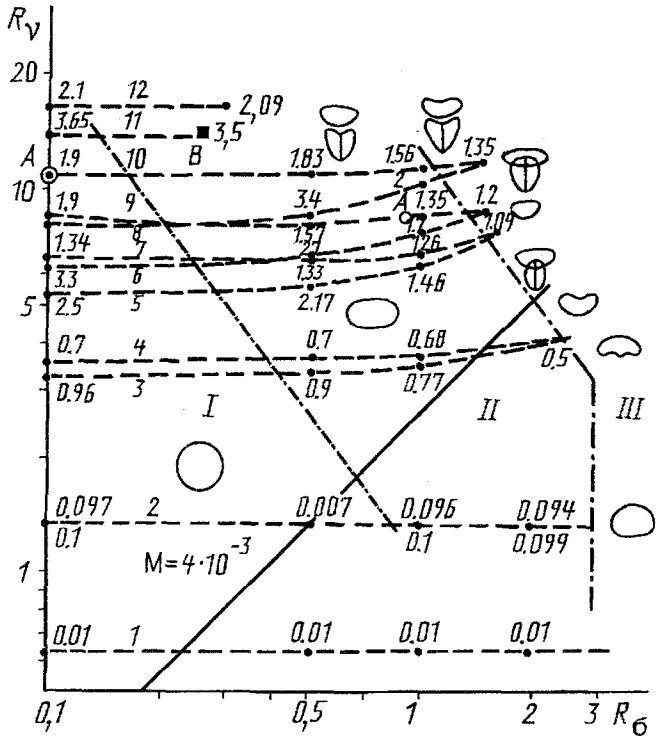

Fig. 11. Chart of the flow modes of a rising drop and the lines of the constant Reynolds numbers Re_1 and Re_2 (A, the appearance of secondary flows behind a drop):

No. of curve	1	2	3	4	5	6	7	8	9	10	11	12
Re_1	0.4	0.4	40	0.4	60	60	0.4	60	0.4	0.4	20	0.4
Re_2	0.1	1	12	12	40	60	40	100	60	100	200	200

In this case, there occurs a jump in the resistance coefficient: $Cd = 0.69$ which is 16% smaller than Cd for a solid sphere (it was higher by 27%). The pressure on the external surface of the drop changes substantially over the entire boundary: the viscous forces acting on the drop change appreciable in magnitude and direction. These arguments cannot, of course, be considered as the solution for the development of the process in physical time, since they correspond to the development in fictitious time. But since in experiments we observe a rise in the form of a series of jerks (see review [4] and the literature cited there), they provide indirect information on the possible processes accompanying the rise of drops.

An increase in Re_1 corresponds to less viscous media of the drop and to a decrease in shear stresses on the surface. This leads to a reduction in the region of secondary flow which at $Re_1 = 4$ is no longer present ($Re_2 = 200$). From Table 1 it is seen that already at $Re_1 = 60$ the resistance coefficient for $Re_2 > 1$ differs from Cd for a bubble by 8-12% (on the order of the value of ρ_1/ρ_2). From solutions at $Re_2 = 12$ it follows that the difference in Cd for $Re_1 = 40$ and 100 is very insignificant; therefore, in what follows we do not consider $Re_1 > 60$. In Fig. 10b the flow is shown near a deformed drop (the case of a bubble). There is an intense vortex within it. Its center is located near the boundary of the drop. The maximum liquid velocities inside and outside of the drop are nearly equal. As Re_1 decreases at a fixed Re_2 the motion inside of the drop slows down, virtually coming to a halt when $Re_1 < 0.1$.

Calculations for $Re_2 \leq 1$ give approximately the same values of Cd for different Re_1 numbers. The flows depends little on the drop medium. This is not surprising, since the solution of the Euler equations (Hill's spherical vortex [61]) is also an exact solution of the Stokesian approximation of the stationary Navier-Stokes equations [62,

63]. Thus, the same functions make both the convective terms of the full Navier-Stokes equations and viscous terms vanish [24]. Therefore, the solutions of the full Navier-Stokes equations at small Re_2 values must not strongly depend on Re_1. The coincidence of the resistance coefficient with the data for a solid sphere is explained by the statement of boundary conditions at "infinity" that correspond to a nonperturbed flow at a finite distance from the sphere. A comparison of solutions for different boundary conditions and distances from the bubble [26] shows that the conditions of nonperturbed flow give values of Cd 20-25% higher than those obtained under the Oseen-type condition which takes into account the presence of a wake behind a bubble [60]. This gives better agreement with experimental data.

Thus, at $Re_1 = 0.4$, $Re_2 = 0.1$, We = 0.0004 (Fr = 0.009, $R_\sigma = 0.15$; $R_\nu = 0.65$, $M = 1.4 \cdot 10^{-4}$, $M_{dr} = 10^{-9}$) there is an intense vortical motion in the interior of the drop whose maximum velocity is commensurable with the drop rise velocity. The solutions obtained for $Re_2 < 1$ with $Re_1 = 0.4$ and 60 correspond to the rise of liquid drops whose parameter M_{dr} is smaller than M for the surrounding medium, since the M_{dr} to M ratio is the same as for $Re_2 > 1$; $Re_1 > 2$ is the case of a "bubble" (at $Re_1 = 0.4$, $Re_2 > 1$ is the case of a "solid sphere," since the value of M_{dr} exceeds M of the external medium). To obtain solutions with M_{dr} higher than M at small values of Re_2 and to compare them with the solution for a solid sphere, we must solve the internal problem with Re_1 smaller than Re_2. For a fixed Re_2 number the values of M_{dr} change by more than seven orders of magnitude if $Re_1 = 0.4$-60: $M_{dr}=2(\rho_1/\rho_2)^3(Re_1/Re_2)^4M$. Note that for water $M \approx 10^{-11}$, for mineral oil $M \approx 0.01$, and for syrup $M \approx 10^6$ [50].

3.4. Rise of strained drops

As We increases at fixed Reynolds numbers, drops flatten in the direction of rise. The change in the surface (in the transverse to longitudinal dimension ratio of a drop) reaches 3% at We $\approx$ 0.24 for different values of Re_1 and $Re_2 \geq 1$. On the diagram with coordinates R_σ and R_ν this is region I (Fig. 11). When $Re_2 \leq 1$, the flow pattern and the degree of boundary warping are identical for $0.4 \leq Re_1 \leq 60$, but for large Re_2 numbers the differences are already evident. Thus, the upper end of the straight line which corresponds to the boundary of region I at $Re_1 = 0.4$ shifts somewhat more rightward, with the values of We increasing insignificantly in this case.

The dashed lines in Fig. 11 present calculations of We at fixed Re_1 and Re_2 numbers. At small values of Re_2 the data for $Re_1 = 60$ and 0.4 virtually coincide. The figures at the points on the lines indicate the values of Fr obtained in the solution. The difference of this diagram from the previous one for a bubble on which the isolines of Fr were depicted should be emphasized. The presence of still another independent parameter characterizing the medium of the drop requires carrying out a great number of calculations for constructing diagrams with the prescribed value of M_{dr}. Of course, Fig. 11 does not permit one to easily plot the dependences of the drop rise velocity on its size in various liquids, but it discloses the main effects of the process of rise. Thus, at a fixed Re_2 number, $Re_2 > 1$, and at different Re_1 numbers the points corresponding to the same values of R_σ come closer together (curves 3 and 4, 5 and 7, 6 and 9, 8 and 10 converge) with an increase in R_σ. The values of Fr also equalize in this case. This indicates that the rise velocities of drops of the same size become identical in spite of the fact that the M_{dr} values on these curves differ by more than seven orders of magnitude. The shape of drops varies from a sphere to a flattened ellipsoid on the right boundary of region II denoted by a broken dash-dotted line. The flow patterns are very diversified in this case (shown schematically in the diagram).

Thus, when $Re_2 \leq 1$ the curves corresponding to $Re_1 = 0.4$ and 60 virtually coincide (just as the Froude numbers on them). The shape of the drops differs little from a sphere, and only when $R_\sigma > 1$ does flattening appear on the back side, and the "corner" on the surface becomes evident. At $Re_1 = 0{,}4$, $Re_2 = 1$, We = 1.62 (Fr = 0.09, $R_\sigma = 2.94$, $R_\nu = 1.39$, M = 91, $M_{dr} = 3.56$) there is an intense vortex within the drop, and the maximum velocity is comparable with the rise velocity. The resistance coefficient is the same as for a solid sphere, whereas the flow within the sphere corresponds more to the case of a gas bubble, as in Fig. 10b (in this case $M_{dr} < M$). This seeming disagreement can be simply explained if we remember that for $Re_2 \leq 1$ the solutions depend little on Re_1, while the motion in a drop is described by the solution given in [61]. Since the value of Fr is very small (creeping flow, small rise velocity), the Archimedes force component, proportional to $-\cos\theta/Fr$, will prevail in the determination

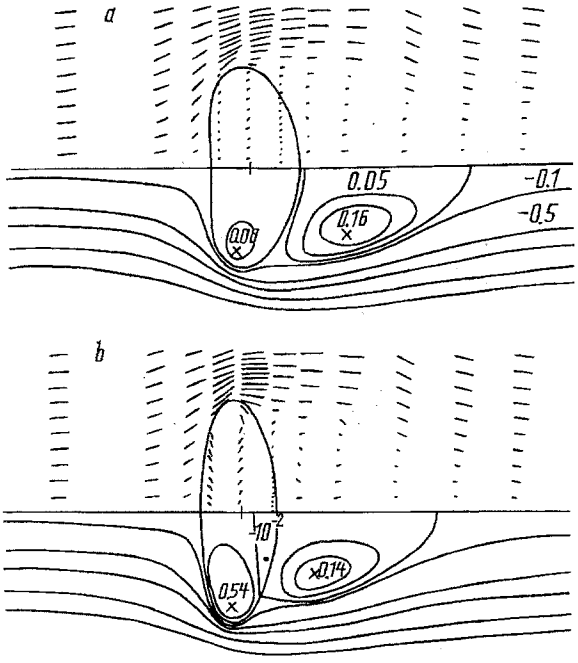

Fig. 12. Flow pattern near a rising drop: a) $\rho_1/\rho_2 = 0.1$; $Re_1 = 0.4$, $Re_2 = 100$, We = 5.2, $M = 2.1 \cdot 10^{-6}$, $M_{dr} = 8.2$; b) $\rho_1/\rho_2 = 0.1$, $Re_1 = 60$, $Re_2 = 100$, We = 5.56, $M = 2.6 \cdot 10^{-6}$, $M_{dr} = 2 \cdot 120^{-3}$.

of the form for the function of the pressure p_1 and, consequently, also of the friction on the boundary. The pressure p_2 on the surface from the side of external flow increases monotonically in motion from the nose to the rear. Starting with a certain value of We (already at We = 1.6204 and $R_\sigma = 3.18$) substantial changes occur in the motion of the liquid. The intensity of the vortex in the drop increased by almost a factor of 2 and the velocity profile became nonmonotonous over the sections in the external flow on the back side; nonuniformity appeared in the vicinity of the pressure "corner." The Fr value fell to 0.08 (in that case M = 106.6 and $M_{dr} = 4.16$). For higher values of We the boundary of the drop changed in a wave-like fashion, and no stationary solution was obtained.

With $Re_2 \leq 0.1$ and different Re_1 and We numbers the shape is practically spherical. When $R_\sigma \geq 3$, we failed to obtain a developed flow pattern.

When $Re_2 > 1$, the rise velocity depends substantially on the drop medium. In the course of strain (increase in We) these differences become smaller, and they virtually disappear at We $\approx$ 3.5 - 4.2 for Re_2 = 1 - 40. The upper part of the broken dash-dotted line, which separates regions II and III in Fig. 11, corresponds to We $\approx$ 4 - 4.5 for $Re_2 > 40$. This segment is constructed from the values calculated for the case where a vortex wake appears behind a drop (when $Re_1, Re_2 \geq 40$) or a wavy boundary appears on the back side of the drop at smaller Re_2 numbers.

Thus, at $Re_1 = 40$, $Re_2 = 12$, We = 6.1 (Fr = 0.45, $R_\sigma = 2.6$, $R_\nu = 4.3$, M = 0.049, $M_{dr} = 3.9 \cdot 10^{-7}$) free stream flow around a drop is still nonseparating. Thre drop is flattened, its front surface is smooth, and the back one is wavy. There is an intense vortex within it with the "center" near the edge of the drop. The velocity profile in the middle section is virtually uniform and its value is much smaller than the rise velocity. With a further increase in We, the wave in the lower portion becomes stronger and a stagnant zone appears in the cavity near the edge [57] (just as in the case of a bubble (see Fig. 4), the rise medium and the drop size are almost the same). However, in contrast to the bubble, no spacious vortex wake was formed here behind the drop. Thereafter, in iterations the boundary of the back zone varies in a wave-like fashion.

Solutions at $Re_1 = 0.4$ and $Re_2 = 12$ up to We = 3.4 ($R_\sigma = 1.9$) have the symmetrical shape of a flattened ellipsoid. But already at We = 3.48 (Fr = 0.48, $R_\sigma = 1.91$, $R_\nu = 4.22$, M = 0.0086, $M_{dr} = 6.2$) the number of iterations increases dramatically in the course of finding stream functions, the entire surface of the drop becomes wavy, its front side curves inward, and no steady flow is obtained.

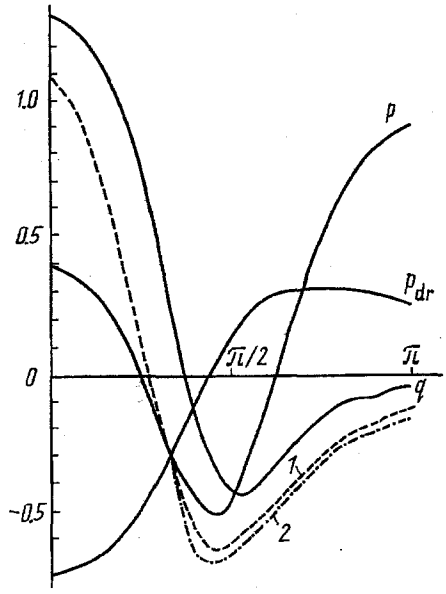

Fig. 13. Graphs of the functions of the pressure on a spherical drop: $\rho_1/\rho_2 = 0.1$, $Re_1 = 0.4$, $Re_2 = 200$, $We = 0.04$, $M = 1.3 \cdot 10^{-13}$, $M_{dr} = 10^{-7}$; 1) calculation for a solid sphere [67]; 2) solution in [66].

TABLE 2. Correspondence Between Hydrodynamic and Geometric Characteristics

Re_1	Re_2	$R_\sigma = 0.2$		$R_\sigma = 0.5$		$R_\sigma = 1.0$		$R_\sigma = 1.5$		We	χ
		We	χ	We	χ	We	χ	We	χ		
0.4	0.1									0.18	1
0.4	1									1.6	1.1
40	12	0.08	1.01	0.48	1.05	1.5	1.2	2.9	1.5	5.76	2
0.4	12	0.08	1.01	0.32	1.03	1.28	1.16	2.6	1.5	3.44	2
60	40	0.18	1.02	1.08	1.15	2.95	1.57	4.9	2.17		
60	60	0.24	1.03	1.36	1.2	3.45	1.8			5	2.4
0.4	40	0.12	1.01	0.68	1.06	2.5	1.3			3.8	1.6
60	100	0.34	1.04	1.72	1.28	4.2	2.2			5.5	2.9
0.4	60	0.15	1.01	0.8	1.07	2.7	1.36			4.6	2.1
0.4	100	0.16	1.01	0.92	1.08	3.2	1.42			5.2	2.1
20	200	0.28	1.03								
0.4	200	0.18	1.01							0.4	1.03
20	100	0.32	1.03	1.52	1.22					3.5	1.8

At larger values of Re_2 (< 60) and small Re_1 the drops also undergo deformation with rise in We up to We ≈ 3.45 in a wedge-like fashion with a "droplet" on the back side. Up to We = 3.85 ($Re_1 = 0.5$, $Re_2 = 45$, Fr = 1.1, $R_\sigma = 1.32$, $R_\nu = 7.6$, $M = 2.6 \cdot 10^{-5}$, $M_{dr} = 2.6$) the intensity of motion in the drop is small (the stream function maximum is equal to ~ 0.17), and the external flow is nonseparating. We were unable to proceeed further along We, since the surface of the drop on its rear side varies in waves in iterations when the shape of the drop is calculated. For large Re_1 number the shape of the drop is symmetrical up to We = 3.45; with a further increase in We it becomes asymmetrical, and starting with We = 4.5 a vortex wake appears behind it. Simultaneously, within the drop on its back side a "buffer" vortex appears (the "droplet" virtually forms a stagnant zone), which rotates in the opposite direction from that of the former vortex. Thus, the three vortices form a system hydrodynamically compatible with the external flow, with the point of contact between them on the drop surface: $Re_1 = 69$, $Re_2 = 45$, We = 4.95 (Fr = 1.1, $R_\sigma = 1.5$, $R_\nu = 7.85$, $M = 5 \cdot 10^{-5}$, $M_{dr} = 9.7 \cdot 10^{-9}$, and the stream function maximum in the

interior of the drop is equal to ~ 0.6). As We increases, the zones of vortex flow in the external medium and within the drop on its back side grow.

At $Re_2 = 60$ the distance between curves 6 and 9 corresponding to $Re_1 = 60$ and 0.4 (see Fig. 11) increases. This means that the liquid viscosity of the drop exerts a substantial effect on the rise (the density ratio remained invariant). At a certain value of We, a zone of secondary flow is formed behind the drop ($Re_1 = 0.4$) at a certain distance from it. The intensity of the vortex motion both inside and outside of the drop is small. As We rises, the drop flattens, the zone of secondary flow behind it grows, and a depression appears on its upstream side in transition to region III. The flow with We = 4.62 (Fr = 1.19, $R_\sigma = 1.4$, $R_\nu = 9.1$, $M = 1.3 \cdot 10^{-5}$, $M_{dr} = 6.58$) has the same structure as that in Fig. 12a. At $Re_1 = 60$ the symmetry of the shape is preserved up to the formation of a vortex on the downstream side (We = 4.55) and further with an increase in We. For We = 4.97 (Fr = 1.22, $R_\sigma = 1.43$, $R_\nu = 9.02$, $M = 1.58 \cdot 10^{-5}$, $M_{dr} = 1.55 \cdot 10^{-8}$) the flow pattern is the same as in Fig. 12b.

Calculations for $Re_2 = 100$ already near spherical drops give different patterns of flow of the external liquid (lines 8, and 10 in Fig. 11). At $Re_1 = 0.4$ there is a secondary flow behind the drop not contacting the latter. As We grows, the drop flattens, its front part being flatter, and the region of the secondary flow behind it increases. At We $\approx$ 4.5 a depression appears in the front part of it. In Fig. 12a (We = 5.2, Fr = 1.37, $R_\sigma = 1.38$, $R_\nu = 12.19$) we have a picture with a developed vortex flow behind the drop whose intensity already exceeds that of the internal vortex.

At $Re_1 = 60$ the flow is nonseparating, and the shape of the drop is symmetrical up to We $\approx$ 4.3. A closed vortex wake appears at We = 4.34 (simultaneously one other vortex appears within it on the back side). As We grows, the vortex behind the drop increases in size (Fig. 12b, We = 5.56, Fr = 1.35, $R_\sigma = 1.43$, $R_\nu = 12.25$). The effect of the composition of the drop medium on the process of the rise of the drop and its shape is illustrated in Fig. 12. The M values of the liquid of the drop differ by more than seven orders of magnitude, whereas the R_σ and R_ν values are nearly equal, i.e., the external medium is practically the same, just as the dimensions of the drop. The rise velocities of drops are the same, but the flow structures differ substantially.

Finally, let us make comparisons of the function of the pressure p. The recovery of pressure for Navier-Stokes equations even in the regions with known boundaries is not a simple problem, since the equations themselves incorporate only the first derivatives of p. Thus, there is a certain arbitrariness in the specification of the additive function of time, which is often selected by fixing p at a certain point in the flow region. In the case of a free surface problem the function of the pressure p is contained in the boundary condition for normal stresses and, thus, the addition to pressure influences the size of the flow region. The means of selecting a constant in the pressure function were discussed in [6, 25, 26, 43] for stationary problems and in [64, 65] for the problem of flow behind a drop. Therefore, when comparing the results of calculations with the solutions of the problem of flow even around a solid sphere, it should be borne in mind that there may be a discrepancy in the function of p accurate to the shift in the graph. The calculation of the problem of rise, i.e., the selection of the Froude number, which is a factor in the term responsible for the presence of gravity, leads to additional deviations. In this regard the function of the generalized pressure q, which is generally recovered in calculations in the regions with known boundaries, is the best choice for carrying out comparisons. In Fig. 13 pressure curves are given corresponding to the case of a "solid sphere" ($R_\sigma = 0.12$, $R_\nu = 16.8$, Fr = 2.11). The symbols p and p_{dr} designate the pressure graphs on the drop boundary outside and inside of Γ; q is the generalized pressure of the external liquid on Γ. There is qualitative coincidence with calculations of works [66, 67] for flow around a solid sphere.

Pressure graphs for $Re_2 = 100$ ($Re_1 = 0.4$, We = 0.08, Fr = 1.88, $R_\sigma = 0.14$, $R_\nu = 11$) have the same character; the amplitude decreases almost two times.

In the case of a "spherical bubble" ($Re_1 = 60$) the pressure functions agree well with the calculations given in [60]. The greatest differences ($\approx$ 20%) are observed at the front point. The function p_{dr} is small, practically constant, and changes sign from minus to plus in the vicinity of $\theta = \pi/2$. The deformation of a drop, the appearance of a vortex wake behind it, leads to the appearance of the "peak" in the pressure at the "edge" of the drop. On the plane surfaces of the drop the pressure is virtually constant.

The correspondence between the hydrodynamic values of the parameters and the geometric characteristic of the drop χ is demonstrated in Table 2.

3.5. Generalization of results

Calculations of the flow around spherical drops with different Re_1 numbers and prescribed $Re_2 > 1$ reveal two limiting cases for the state of the drop: at $Re_1 = 0.4$ a solid surface can be virtually simulated (here, as a rule, $M_{dr} > M$; at $Re_1 = 60$ the results are close to the solutions for a rising bubble and can serve as a model for a vapor bubble (in this case $M_{dr} < M$). The estimate obtained for Re_1 remains valid for different values of Re_2: the media both within the drop and outside it change, but the "bubble" and "solid sphere" approximation is preserved for the indicated Re_1 values. In this case the M values for the media differ by eight orders of magnitude. To increase this difference at a fixed Re_2, it is necessary either to lower Re_1, which does not give substantially different results (the data are close to the results for a solid sphere), or to increase Re_1 which also does not give new data since there is a bubble in the limit. Thus, if in the media of the drop and external liquid the M values differ by eight (and more) orders of magnitude, then we may regard one with respect to the other to be either solid or gaseous (it should, of course, be borne in mind that here the fixed value is $\rho_1/\rho_2 = 0.1$). Calculations at $Re_2 = 60$ and 200 with $Re_1 = 4$ indicate that at this value of Re_1 the solutions reflect to a greater extent the properties of the bubble than of a solid particle. In the interior the maximum velocity is equal to about half the bubble rise velocity, and the region of secondary flow behind it is absent, as seen in Fig. 10a.

As the drop undergoes deformation and transforms into a "pancake" the intensity of motion inside it (as compared with the external flow velocity) decreases, concentrating on the edges of the drop.

The inclined lines between regions I and II, II and III (see Fig. 11) were drawn based on the results of calculations with $Re_1 = 60$. They lie somewhat higher than the corresponding lines in Fig. 9 for a rising bubble. The difference between the values of Fr at corresponding points of the diagrams for strained drops (the case of a "bubble") and bubbles reaches 50% (they differ several times with a decrease in Re_1). With transition to region III, when a wave appears, the difference decreases to 20%. In this case the medium and its motion do not virtually influence the value of Fr. The shape of the drops and the flow structure are different. This means that the drop rise velocity is determined by the density ratio of the media, i.e., by the buoyancy force. From the aforegoing it follows, in particular, that separation or a secondary flow makes the main contribution to the resistance of a drop. However, different flow patterns near the drop surface exert a substantial effect on the heat and mass transfer characteristics.

Separation on a drop can occur only after the formation of a new vortex in its interior. For this to happen, it is necessary that a rather intense vortex motion must exist behind the drop in the stagnation zone capable of developing flow on a portion of the surface and establishing conditions for a new "buffer" vortex within it. For liquids with $M_{dr} < M$ (and, as a rule, with $M_{dr} < 4 \cdot 10^{-3}$) this is observed already with $Re_2 > 40$. For $Re_2 < 40$ and large We numbers unsteady oscillations are observed on the back side of the surface. If the medium of the drop and the external medium are such that $M_{dr} > M$ (as a rule, $Re_1 < Re_2$ for a fixed $\rho_1/\rho_2 < 1$), then at large Re_2 numbers the region of secondary flow appears behind the drop and it does not close directly on the drop boundary.

The curves for different Re_1 values and a fixed value of Re_2 merge at the same We number when a depression appears at the front of the drop at small Re_1 values and a vortex wake forms at high values of Re_1 (the secondary flow behind the drop at $Re_1 = 0.4$ appears earlier). The lines Fr = const for a constant value of M_{dr} are of the same character as for a bubble, and the inclined line between regions II and III in Fig. 11 lies in the vicinity of the points of tangency of straight lines representing the surrounding medium with the isolines of Fr. Thus, in media with small M the dependence of the rise velocity of the drop of a given liquid on its size has a local maximum which precedes the onset of a vortex wake behind the drop. In media with $M > 10^{-4}$ unsteady oscillations appear on the back side with an increase in the drop size (separation or a secondary flow has not originated as yet). The indicated features are observed in the region with We ≈ 4-4.5. Numerous experiments show [68] (see also review [4]) that the oscillations of the drop surface take place precisely at these values of We.

Just as for a rising bubble, the formation of a vortex wake behind a drop makes the rise velocity independent of one of the hydrodynamic parameters: of R_ν at small M values ($M < 0.004$) and of R_σ at large M values. Thus, the appearance of a vortex behind the drop (for small values of M_{dr}) and a depression in the drop in its front part

(for values of M_{dr} relatively large with respect to M) leads to the self-similarity of its rise velocity both with respect to the drop medium and with respect to one other hydrodynamic parameter, i.e., R_σ or R_ν. In the region of spherical drops (I) there is self-similarity with respect to R_σ, whereas for $Re_2 \leq 1$, also with respect to M_{dr}.

At large Re_2 numbers, the path of the drop rise does not constitute a straight line. This is explained by the formation of a vortex wake behind the drop which in low-viscosity liquids (small M) leads to the loss of stability in the linear rise. Another reason for the unsteady rise is the motion of the medium in the drop. At large Re_2 numbers the intense rotation in the region of the secondary flow behind the drop and the rotational motion inside it form, on a portion of the boundary, a flow with opposing velocities on the different sides of the surface. Such hydrodynamic flows even in the case of a flat surface in the same liquid are unstable [24] and lead to the onset of waves on it. This, in particular, can be the reason for the wavy motion at the back side of the drop in transition to region III at small Re_2 values when a vortex wake originates. Flows of stable types can exist only on formation of a "buffer vortex" which eliminates the source of perturbations. Calculations at Re = 200 provide a qualitative explanation for the unsteady processes during the rise of bubbles in distilled water and alcohol [50] (they precede the region of the local maximum in the rise velocity). In view of this, the hypothesis advanced by Levich [69] that the motion of a gas in a bubble exerts a substantial effect on its fragmentation merits attention. The collapse of the bubble can be caused not by the effects of gas motion proper, which are really not large, but rather the instability mechanisms triggered and sustained by them.

The presence of surfactants or admixtures accumulating on the boundary creates additional friction varying along the surface. Allowance for the motion of the medium in the bubble makes it possible to simulate the influence of surfactants. In fact, at small values of ρ_1/ρ_2 we have a light low-intertia medium in the bubble. By assigning Re_1 we may change the value of friction on the interface between the media. As Re_1 falls, with other parameters fixed, the value of Fr decreases; in the diagram of Fig. 11 the corresponding point lies higher (see, e.g., curves 3 and 4 corresponding to $Re_1 = 40$ and 0.4). As R_σ (or We) grows, the curves for different values of Re_1 get closer, the values of Fr on them equalize (Fig. 11), and with the appearance of the vortex wake or secondary flow on the rear the differences in the rise velocity virtually disappear. All this occurs, as a rule, when $R_\sigma > 1$. On the other hand, it is known that tiny bubbles rise following the Stokes law for a solid sphere. Only with deformation and increase in the volume does transition to the Hadamard-Rybczinsky solution occur. This can be explained by the hypothesis about the presence of surfactants and admixtures in liquids. The hypothesis is corroborated by applying special purification measures, but the reasons for the transition are not revealed. According to the estimates [41], rising individual bubbles of size larger than the capillary constant ($a > \delta_\sigma$ or $R_\sigma > 1$) do not experience the effect of surfactants irrespective of the type of liquid. By comparing calculated and experimental data, we can give the following explanation for the transition of the Stokesian mode of flow to the Hadamard-Rybczinsky solution. Admixtures and surfactants on the surface of a bubble or a drop create a film which changes the magnitude of friction there. The greatest effect is exerted on the back side where the admixtures are swept to. The formation of separation on the surface and of a stagnant zone behind a bubble or a drop erases the individual features of friction associated with the presence of admixtures. The pattern of flow changes and this makes the main contribution to the resistance coefficient.

Finally, we shall make some comparisons with experiments. Points 1 and 5 in Fig. 9 correspond to the points of the local maximum in the graph of the function of the rise velocity on the bubble size for water and for a solution of methyl alcohol [50] (Fig. 8) in which the effect of surfactant is noticeable. It is precisely in this region that the appearance of some unsteady processes is observed, which is associated with the turn of the flow on a portion of the boundary and formation of separation from the drop surface (calculations with $Re_2 = 200$ and $Re_1 = 0.4$).

For other liquids (see 2, 6, 7 in Fig. 9) with higher values of M or small M values and small surface tension coefficient (points 3, 4), the points of local maxima or inflection in the rise velocity graphs correspond to the line pointing to the presence of a vortex wake behind a bubble.

In liquids (8, 9 in Figs. 8 and 9) the inflection points in the bubble rise velocity correspond to the formation of a vortex behind a drop at large Re_1 numbers simulating the case of a "bubble" (see Fig. 11). They lie in the vicinity of the line between regions II and III which is constructed on the basis of such symptoms as are the

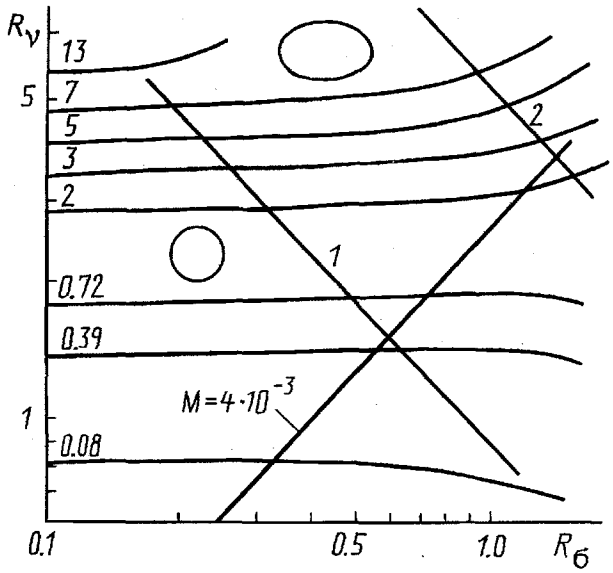

Fig. 14. Chart of flow modes and the isolines of the Froude number of a rising chain of identical bubbles ($L = 6$).

appearance of a vortex wake or a depression in the front part and the presence of a secondary flow behind a drop. According to calculations in the vicinity of this straight line the lines at the level of Fr = const contact the straight lines depicting the surrounding medium and, consequently, the rise velocity here has a local maximum or an inflection point. Thus, here one observes the effect of motion of the bubble medium on the rise.

Solutions at $\rho_1/\rho_2 = 0.5$ predict similar trends in the deformation of the surface and flow structure. At identical Re_1, Re_2, and We numbers we obtain smaller values of Fr than at $\rho = 0.1$ [56], whereas the lines of constant values of Re_1 and Re_2 are located higher than the corresponding lines in Fig. 11. Thus, the entire diagram of flow modes at $\rho = 0.5$ shifts upwards. As is seen from the coupling between M and M_{dr} (Sec. 3.3), in this case we obtain the solution for the liquid of the drop with higher values of M_{dr} than at $\rho = 0.1$ for the same surrounding medium.

Chapter 4. RISE OF A CHAIN OF BUBBLES

Investigation of the rise of a chain of identically sized bubbles moving one after the other represents a still more complex problem than the rise of a single bubble. An indication of the complication of the problem is the presence of one extra independent dimensionless parameter which is the distance between the centers of neighboring bubbles. But this is not the sole complication. Simulation of the effect of neighboring bubbles by stating periodic conditions connects stream functions and their derivatives on different parts of the flow region boundary. In a spherical coordinate region connected with the "center of mass" of the considered bubble, these parts turn out to be located on one side of a curvilinear quadrangle depicting the flow region. In this case the familiar method of realizing the conditions of periodicity - the cyclic pivot method [70] - is unsuitable. An algorithm was developed which exactly realizes the conditions in the iterations of calculation [65].

Experimental investigation becomes very complicated with increased rise velocities. At smaller velocities the dimensions of bubbles decrease, and the visualization of flows becomes practically impossible due to optical distortions. In this regard only the measurement of rise velocity [71, 72] is realizable in practice. To these works we may add recent pool boiling investigations [73], investigations in pipes with an ascending liquid flow [74], and those on the rise velocity in capillary tubes [75]. It seems that the fullest evidence was obtained by the authors of work [74] who measured the longitudinal velocity vector components along the tube section behind a bubble and friction on the walls.

The solution of the periodic problem of flow around a chain of equally spaced identical bubbles makes it possible to determine more precisely the effect of the deflection of boundary conditions from "infinity" to the final

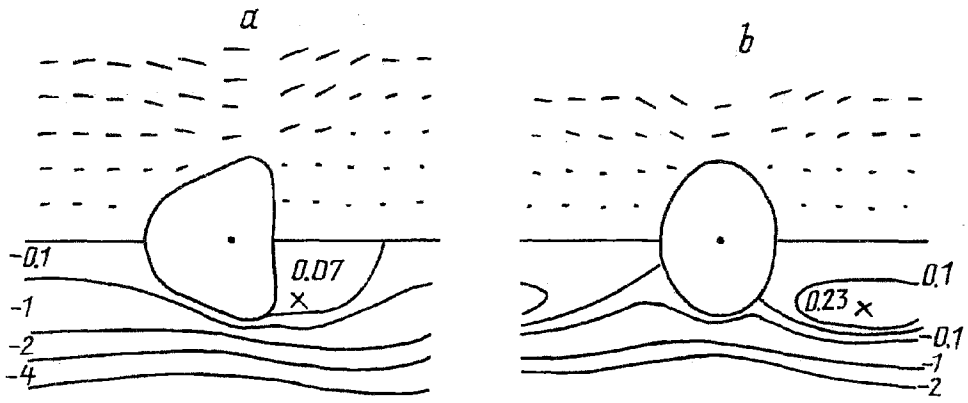

Fig. 15. Flow patterns near bubbles in a chain ($L = 6$): a) Re = 21, We = 13.8, M = 0.011; b) Re= 60, We = 7.6, M = $1.4 \cdot 10^{-5}$.

distance from the bubble during the rise of a single bubble. At $L = 20$ (the distance between the centers of bubbles is $2L$) the flow patterns are identical up to Re = 20. When Re ≥ 40, the vortex wake is much longer: we can distinguish in it the separation region adjoining the bubble surface, and in the wake, the secondary flow zone with closed streamlines. In this case comparison of the results on the resistance coefficient with the predictions for a single bubble [26] shows good agreement (Cd is calculated from flow functions near a body; if the separation point and the bubble shape are determined rather accurately, there is good correspondence between Cd values). The differences become appreciable when the perturbations from the front bubble reach the next bubble. At $L = 10$, starting with Re > 20, the wake of the front bubble closes on the surface of the subsequent bubble and, thus, not a chain of separate bubbles rises, but rather a certain entity of bubbles with liquid in between. The rise velocity of such formations is somewhat higher than that of a single bubble [65], and it is determined by the overall Archimedes force of bubbles. But already at $L = 6$ the Froude numbers at the corresponding points in the diagrams are much higher (Fig. 14). Here line 2 point to the fact that the wake from the front bubble closed on the surface of the subsequent bubble. Characteristic shapes and structures of flows are shown in Fig. 15.

At $L = 4$ (the distance between the bubbles is equal to the diameter) one fails to obtain stationary solutions even for spherical bubbles. In the iterations of calculations of the boundary, it oscillates along the path of the rise. This agrees with the investigation [76] into the stability of the motion of bubbles in an infinite chain.

CONCLUSION

An analysis of the problem concerning the interaction of moving single formations (bubbles and drops) with the surrounding carrying medium shows the possibility of describing real physical processes within the frameworks of the models of ideal and viscous liquids. Generalization of experimental and theoretical data is made by constructing charts of flow modes. A successful selection of the dimensionless numbers R_σ and R_ν as coordinates made it possible to arrange in an ordered fashion in the diagram all of the media by means of the parameter M, with the data for each specific medium being located on a certain straight line whose slope is determined by M. Vast computational data both of the present author and of other investigators for the region of small and intermediate values of dimensionless parameters, converted into the R_σ, R_ν functions, made it possible to fully display the region inaccessible for investigation when the effect of all the parameters is significant and their number cannot be reduced. The use of these very parameters for correlating the data of the problem of steady rise of a drop made it possible to simply demonstrate the influence both of the presence of the medium itself and its motion on the drop rise. Comparison of the data with the problem of bubble rise can be made by simple superposition of diagrams. The logical clarity of the parameters R_σ, which is equal to the ratio of the equivalent radius a of a bubble (drop) to the capillary constant of the surrounding medium δ_σ, allowed the determination of a certain critical size a after which waves appear on the surface at the back side of the bubble (drop) when the value of a is higher than $2\text{-}3\delta_\sigma$. Another form of instability of steady rise is associated with the formation of a stagnant zone and with the

separation of flow from the surface of a bubble or drop characteristic for surrounding media with small values of M. The use of the parameters R_σ and R_ν will definitely significantly simplify the analysis of more complex problems, for example, the problems of the motion of bubbles and drops in tubes with liquid and also the change in the external conditions (reduced or increased gravitation).

REFERENCES

1. I. O. Protodiyakonov and I. E. Lyublinskaya, Hydrodynamics and Mass Transfer in Gas-Liquid Systems [in Russian], Leningrad (1990).
2. I. O. Protodiyakonov and S. V. Uliyanov, Hydrodynamics and Mass Transfer in Disperse Liquid-Liquid Systems [in Russian], Leningrad (1986).
3. O. V. Voinov and A. G. Petrov, Itogi Nauki Tekhniki, Mekh. Zhidk. Gaza, **10**, 86-147 (1976).
4. A. L. Gonor and V. Ya. Rivkind, Itogi Nauki Tekhniki, Mekh. Zhidk. Gaza, **17**, 86-159 (1982).
5. L. V. Ovsyannikov, in: Some Problems of Mathematics and Mechanics, Leningrad (1970), pp. 209-222.
6. V. V. Pukhnachev, Problems with Free Boundaries in Navier-Stokes Equations, Doctoral Dissertation (Phys.& Math. Sciences), Novosibirsk (1974).
7. V. Ya. Rivkind, Hydrodynamics and Heat/Mass Transfer of Drops, Author's Thesis of Doctoral Dissertation (Phys. & Math. Sciences), Leningrad (1986).
8. Rayleigh, Phil. Mag. (6), **34**, 94-99 (1917).
9. O. V. Voinov and V. V. Voinov, Dokl. Akad. Nauk SSSR, 221, No. 3, 559-562 (1975).
10. P. K. Volkov, B. G. Kuznetsov, and Kh. I. Khristov, Chisl. Metody Mekh. Splosh. Sredy (Novosibirsk), **11**, No. 2, 22-23 (1980).
11. I. Cammel, Lecture Notes in Physics, **47**, 141-163 (1976).
12. C. I. Christov and P. K. Volkov, Theor. and Appl. Mech. (Sofia), **16**, No. 3, 59-67 (1985).
13. V. R. Kogan and V. V. Kuznetsov, Zh. Vychisl. Mat. Mat. Fiz., **29**, No. 6, 844-852 (1989).
14. M. J. Miksis, J.-M. Vanden-Broeck, and J. B. Keller, J. Fluid Mech., **123**, 31-41 (1982).
15. A. S. Noskov, in: Metallurgical Thermal Engineering, Moscow (1974), pp. 133-136.
16. A. G. Petrov, Prikl. Mat. Tekh. Fiz., No. 5, 49-54 (1974).
17. O. V. Voinov, Izv. Akad. Nauk SSSR, Mekh. Zhidk. Gaza, No. 1, 150-153 (1978).
18. P. K. Volkov and Kh. I. Khristov, in: Numerical Methods in the Mechanics of Liquid and Gas, Novosibirsk (1980), pp. 19-26.
19. H. El Sawi, J. Fluid Mech., **62**, No. 1, 163-183 (1974).
20. L. D. Landau and E. M. Lifshits, Theoretical Physics [in Russian], Vol. 6, Moscow (1986).
21. W. Thomson, Phil. Mag., **42**, p. 374 (1871).
22. L. D. Landau and E. M. Lifshits, Theoretical Physics [in Russian], Vol. 7, Moscow (1987).
23. A. Serisawa, I. Kataoka, and I. Michiyoshi, Int. J. Multiphase Flow, **2**, 235-246 (1975).
24. J. Batchelor, Introduction to the Dynamics of Fluids [Russian translation], Moscow (1973).
25. P. K. Volkov, Chisl. Metody Mekh. Splosh. Sredy (Novosibirsk), **13**, No. 1, 44-55 (1982).
26. C. I. Christov and P. K. Volkov, J. Fluid Mech., **158**, 341-364 (1985).
27. L. I. Sedov, Mechanics of Continuous Media [in Russian], Vol. 2, Moscow (1973).
28. T. Z. Harmathy, AIChE Journal, **6**, No. 2, 281-288 (1960).
29. J. R. Grace, Trans. Inst. Chem. Eng., **51**, 116-120 (1973).
30. D. Bhaga and M. B. Weber, J. Fluid Mech., **105**, 61-85 (1981).
31. J. H. C. Coppus and K. Rietema, Chem. Eng. Sci., **35**, No. 6, 1495-1497 (1980).
32. B. Rosenberg, David Taylor model basin, Report No. 727 (1950).
33. H. Angelino, Chem. Eng. Sci., **21**, No. 6, 541-550 (1966).
34. J. F. Harper, In. Adv. Appl. Mech.,**12**, 59-130 (1972).
35. P. L. Kapitsa, Zh. Eksp. Teor. Fiz., **18**, Issue 1, 3-18 (1948).
36. D. V. Moore, J. Fluid Mech., **16**, No. 7, 161-176 (1963).

37. W. L. Haberman and R. K. Morton, David Tayler model basin, Report No. 802 (1953).
38. E. Schmidt, VDI Forschungsheft, No. 365, 1-3 (1934).
39. S. S. Kutateladze and V. E. Nakoryakov, Heat/Mass Transfer and Waves in Gas-Liquid Systems [in Russian], Novosibirsk (1984).
40. S. S. Kutateladze, I. G. Malenkov, and E. A. Chinnov, in: Disperse Systems in Energochemical Processes, Novosibirsk (1982), pp. 3-19.
41. P. K. Volkov and E. A. Chinnov, in: Hydrodynamics and Acoustics of Single- and Two-Phase Flows, Novosibirsk (1983), pp. 5-12.
42. P. K. Volkov, in: Numerical Methods of the Dynamics of Viscous Liquid, Novosibirsk (1983), pp. 96-100.
43. G. Ryskin and L. G. Leal, J. Fluid Mech., **148**, 1-43 (1984).
44. H. Tsuge and S. Hibino, J. Chem. Eng. Jap., **10**, No. 1 (1977).
45. R. A. Hartunian and W. R. Sears, J. Fluid Mech., **3**, No. 1, 27-47 (1957).
46. P. K. Volkov, Hydrodynamics of Rising Bubbles and Drops, Doctoral Dissertation (Phys. & Math. Sciences), Novosibirsk (1992).
47. P. K. Volkov and E. A. Chinnov, Prikl. Mat. Tekh. Fiz., No. 1, 94-99 (1989).
48. D. W. Moore, J. Fluid Mech., **23**, No. 4, 749-766 (1965).
49. B. J. Wu, R. T. Deluca, and Wegener, J. Chem. Eng. Sci., **29**, 1307-1309 (1976).
50. W. L. Haberman and R. K. Morton, Proc. Amer. Soc. Civil Engrs., **49(387)**, 1-25 (1954).
51. D. A. Frank-Kamenetsky, Diiffusion and Heat Transfer in Chemical Kinetics [in Russian], Moscow (1947).
52. I. G. Malenkov, Prikl. Mat. Tekh. Fiz., No. 6, 130-134 (1968).
53. H. Helmholtz, D. Akad. d. Wiss. Berlin, S. 215-228.
54. C. I. Christov and M. D. Todorov, Int. Conf. "Numerical Methods and Applications-84," Sofia (1984), pp. 216-223.
55. V. Ya. Rivkind, Dokl. Akad. Nauk SSSR, **227**, No. 5, 1071-1074 (1976).
56. P. K. Volkov, Modelirovanie v Mekh. (Novosibirsk), **4(21)**, No. 5, 48-74 (1990).
57. P. K. Volkov, Prikl. Mat. Tekh. Fiz., No. 1, 78-88 (1992).
58. G. Schlichting, Boundary-layer Theory [Russian translation], Moscow (1974).
59. A. Tom and K. Aiplt, Numerical Calculations of Fields in Technology and Physics [Russian translation], Moscow, Leningrad (1964).
60. D. C. Brabston and H. B. Keller, J. Fluid Mech., **69**, No. 1, 179-189 (1975).
61. M. J. M. Hill, Phil. Roy. Soc. London, Ser. A, **185**, Pt. 1 (1894).
62. J. Hadamard, Comp. Rend. Acad. Sci., **52**, No. 25, 1735-1741 (1911).
63. M. W. Robczynski, Bull. Int. Acad. Sci. Cracovia, Ser. A, No. 1, 40-46 (1911).
64. V. Ya. Rivkind, Notes of the Scientific Seminar at the V. A. Steklov Leningrad Optomechanical Inst., Vol. 84 (1979), pp. 220-243.
65. P. K. Volkov, Prikl. Mat. Tekh. Fiz., No. 3, 87-91 (1991).
66. Y. Rimon and S. I. Cheng, Phys. Fluids, **12**, No. 5, 949-959 (1969).
67. V. I. Shatrov, "A Method for Calculating a Conducting Incompressible Viscous Liquid Flow around a Sphere at Reynolds Numbers $\leq$ 1000", Preprint 30-84 of the Institute of Theoretical and Applied Mathematics, Siberian Branch of the USSR Academy of Sciences, Novosibirsk (1984).
68. S. Winnikov and B. T. Chao, Phys. Fluids, **9**, No. 1, 50-61 (1966).
69. V. G. Levich, Physicochemical Hydrodynamics [in Russian], Moscow (1959).
70. A. A. Samarskii and E. S. Nikolaev, Methods for Solving Network Equations [in Russian], Moscow (1978).
71. J. R. Crabtree and J. Bridgewater, Chem. Eng. Sci., **24**, No. 12, 1755-1768 (1969).
72. Marx, Proceedings of ASME, Theor. Foundations of Eng. Calculations [Russian translation], **95**, No. 1 (1973).
73. F. Durst, B. Schonung, K. Selanger, and M. Winter, J. Fluid Mech., **170** (1986).
74. V. E. Nakoryakov, O. N. Kashinsky, and B. K. Kozmenko, Int. J. Multiphase Flow, **12**, No. 3, 337-355 (1986).
75. E. A. Chinnov and D. N. Kravshenko, Izv. Sib. Otd. Akad. Nauk SSSR, Ser. Tekh. Nauk, Vyp. 1, 120-124 (1990).
76. F. A. Morrison, Chem. Eng. Sci., **28**, No. 1, 1115-1116 (1973).